

A MULTIPLE MEASUREMENT VECTOR APPROACH TO SYNTHETIC APERTURE RADAR IMAGING

LILIANA BORCEA AND ILKER KOCYIGIT *

Abstract. We study a multiple measurement vector (MMV) approach to synthetic aperture radar (SAR) imaging of scenes with direction dependent reflectivity and with polarization diverse measurements. The unknown reflectivity is represented by a matrix with row support corresponding to the location of the scatterers in the scene, and columns corresponding to measurements gathered from different sub-apertures, or different polarization of the waves. The MMV methodology is used to estimate the reflectivity matrix by inverting in an appropriate sense the linear system of equations that models the SAR data. We introduce a resolution analysis of imaging with MMV, which takes into account the sparsity of the imaging scene, the separation of the scatterers and the diversity of the measurements. The results of the analysis are illustrated with some numerical simulations.

Key words. synthetic aperture radar imaging, convex optimization, multiple measurement vector, simultaneously sparse.

AMS subject classifications. 35Q93, 58J90, 45Q05.

1. Introduction. Sparsity promoting optimization [26, 25, 22, 9, 11, 10, 12] is an important methodology for imaging applications where scenes that are sparse in some representation can be reconstructed with high resolution. There is a large body of literature on this topic in synthetic aperture radar imaging [4, 32, 28], sensor array imaging [13, 14, 7], medical imaging [30], astronomy [6], geophysics [33], and so on.

We are interested in the application of synthetic aperture radar (SAR) imaging, where a transmit-receive antenna on a moving platform probes an imaging scene with waves and records the scattered returns [20, 17]. This is a particular inverse problem for the wave equation, where the waves propagate through a homogeneous medium, back and forth between the platform and the imaging scene, and the unknown is modeled as a two-dimensional reflectivity function of location on a known imaging surface. Most SAR imaging is based on a linear model of the data, where the unknown reflectivity is represented by a collection of independent point scatterers [17]. The image is then formed by inverting approximately this linear relation, using filtered backprojection or matched filtering [17], also known as Kirchhoff migration [5]. Such imaging is popular because it is robust to noise, it is simple and works well when the linear model is a good approximation of the data. However, the resolution is limited by the extent of the aperture, the frequency and the bandwidth of the probing signals emitted by the moving platform [20, 17]. The promise of sparsity promoting optimization is that these resolution limits can be overcome when the unknown reflectivity has sparse support [4, 32, 28].

The modeling of the reflectivity as a collection of points that scatter the waves isotropically may lead to image artifacts. It is known that even if the scatterers are small, so that their support may be represented by a point and the single scattering approximation (i.e., the linear data model) can be used, their reflectivity may depend on the frequency and the direction of illumination [2, Chapters 3, 5]. Moreover, the scatterers have an effective polarization tensor that describes their response to different polarizations of the probing electromagnetic waves [2, 3]. Thus, the reflectivity function depends on more variables than assumed in conventional SAR, and the resulting images may be worse than expected. For example, a scatterer that reflects only within a narrow cone of incident angles cannot be sensed over most of the synthetic aperture, so its reconstruction with filtered backprojection will have low resolution. Direct application of sparse optimization methods does not give good results either, because of the large systematic error in the linear data model that assumes a scalar, constant reflectivity over the entire aperture.

SAR imaging of frequency-dependent reflectivities has been studied in [16, 35, 34], using either Doppler effects, or data segmentation over frequency sub-bands. Data segmentation is a natural idea for imaging both frequency and direction dependent reflectivities that are regular enough so that they can be approximated as piecewise constant functions over properly chosen frequency sub-bands and cones of angles of incidence (i.e., sub-apertures). Images can be obtained separately from each data set, but the question is how to fuse the information to achieve better resolution. The study in [8] uses the multiple measurement vector (MMV) methodology [31, 15, 39], also known as simultaneously sparse approximation [38, 37], for this purpose. The MMV framework fits here because the reflectivity is supported at the same locations in the imaging scene, for

*Department of Mathematics, University of Michigan, Ann Arbor, MI 48109-1043.
Email: borcea@umich.edu & ilkerk@umich.edu

each data set. In the discrete setting, this means that the unknown is represented by a matrix \mathbf{X} with row support corresponding to the pixels in the image that contain scatterers, and with columns corresponding to the different values of the reflectivity for each frequency band, sub-aperture and polarization.

The goal of this paper is two-fold: First, we introduce a novel resolution theory of imaging with MMV, that applies to a general linear system. We do not pursue the usual question of exact recovery of the unknown matrix \mathbf{X} , which requires stringent assumptions on the imaging scene that are unlikely to hold in practice. Instead, we estimate the neighborhood of the row support of \mathbf{X} that contains the largest entries of the MMV reconstruction. The size of this neighborhood plays the role of resolution limit and we quantify its dependence on the sparsity of the imaging scene, the separation between the scatterers, the diversity of the data set and the noise level. The second goal of the paper is to explain how the theory applies to SAR imaging. The study [8] is proof of concept that MMV can be used to image direction dependent reflectivities from data gathered over multiple sub-apertures. However, it does not provide a resolution analysis and it does not demonstrate the advantage of using MMV over imaging with a single sub-aperture at a time. In this paper we quantify the improvement brought by the MMV approach and assess the results of the resolution theory for the application of SAR imaging both direction and polarization dependent reflectivities.

The paper is organized as follows: We begin in section 2 with the theoretical results, stated for a general linear system with unknown matrix \mathbf{X} . The application of SAR imaging is discussed in sections 3 and 4. The proofs of the results are in section 5. We end with a summary in section 6.

2. Theory. We state here our main results on the resolution of imaging with MMV. We begin in section 2.1 with a brief discussion on MMV, and then give the results in section 2.2.

We use henceforth the following notation convention: Bold uppercase letters, as in $\mathbf{X} \in \mathbb{C}^{N_{\mathbf{y}} \times N_v}$, denote matrices and bold lowercase letters denote vectors. We also use an arrow index, as in $\mathbf{x}_{j \rightarrow} \in \mathbb{C}^{1 \times N_v}$, to distinguish the rows of \mathbf{X} from its column vectors denoted by $\mathbf{x}_j \in \mathbb{C}^{N_{\mathbf{y}} \times 1}$.

2.1. Preliminaries. Consider a general linear model of a data matrix $\mathbf{D} \in \mathbb{C}^{N_r \times N_v}$,

$$\mathbf{G}\mathbf{X} = \mathbf{D}, \quad (2.1)$$

where the unknown matrix $\mathbf{X} \in \mathbb{C}^{N_{\mathbf{y}} \times N_v}$ is mapped to \mathbf{D} by a given sensing matrix $\mathbf{G} \in \mathbb{C}^{N_r \times N_{\mathbf{y}}}$. In the context of SAR imaging, \mathbf{X} is the unknown reflectivity discretized* at $N_{\mathbf{y}}$ points $\{\mathbf{y}_j\}_{1 \leq j \leq N_{\mathbf{y}}}$ in the imaging region Ω , a bounded set on a known surface. The matrix \mathbf{D} is an aggregate of N_v data sets or views, each consisting of N_r measurements of the wave at the moving radar antenna. The column \mathbf{x}_v of \mathbf{X} is the reflectivity for the v -th view, and the sensing matrix \mathbf{G} is the discretization of the kernel of the integral operator that defines the single scattering approximation of the wave, as described in section 3.

Denote by $\mathcal{S} \subset \{1, \dots, N_{\mathbf{y}}\}$ the set of indexes of the nonzero rows of \mathbf{X} , and suppose that its cardinality $|\mathcal{S}|$ is small with respect to $N_{\mathbf{y}}$. We call \mathcal{S} the row support of \mathbf{X} and let $\Omega_{\mathcal{S}} = \{\mathbf{y}_q, q \in \mathcal{S}\}$ be the set of associated locations in Ω .

When $N_v = 1$, the linear model (2.1) corresponds to the single measurement vector (SMV) problem,

$$\mathbf{G}\mathbf{x} = \mathbf{d}, \quad (2.2)$$

with unknown vector $\mathbf{x} \in \mathbb{C}^{N_{\mathbf{y}} \times 1}$ and data vector $\mathbf{d} \in \mathbb{C}^{N_r \times 1}$, where we dropped the column index 1. This problem has been studied extensively in the context of compressed sensing [26, 25, 22, 9, 11, 10, 12, 29] for the undetermined case $N_r \ll N_{\mathbf{y}}$. In particular, it is known [23, Corollary 1] that if

$$\|\mathbf{x}\|_0 = |\mathcal{S}| < \text{spark}(\mathbf{G})/2, \quad (2.3)$$

where $\text{spark}(\mathbf{G})$ is the smallest number of linearly dependent columns of \mathbf{G} , then (2.2) has a unique solution satisfying (2.3), given by the minimizer of the combinatorial optimization problem

$$\text{minimize } \|\mathbf{z}\|_0 \quad \text{subject to } \mathbf{G}\mathbf{z} = \mathbf{d}. \quad (2.4)$$

The norm $\|\mathbf{z}\|_0$ equals the number of nonzero entries in \mathbf{z} .

*We assume that the $N_{\mathbf{y}}$ points define a fine mesh in Ω , so we can neglect errors due to scatterer locations off the mesh.

This result is generalized in [15, Theorem 2.4] to the MMV problem (2.1) for $N_v > 1$. It states that when the number of nonzero rows in \mathbf{X} , denoted by $\|\mathbf{X}\|_0$, satisfies

$$\|\mathbf{X}\|_0 < [\text{spark}(\mathbf{G}) + \text{rank}(\mathbf{D}) - 1]/2, \quad (2.5)$$

the linear system (2.1) has a unique solution satisfying (2.5), given by the minimizer of

$$\text{minimize } \|\mathbf{Z}\|_0 \text{ subject to } \mathbf{GZ} = \mathbf{D}. \quad (2.6)$$

Thus, if the different data sets bring new information, so that \mathbf{D} has large rank, the MMV problem is uniquely solvable for less stringent conditions on the row support of \mathbf{X} i.e., for less sparse imaging scenes.

The combinatorial problems (2.4) and (2.6) are not computationally tractable, so they are replaced by convex relaxations. The minimizer of the convex problem

$$\mathcal{P}_1: \text{ minimize } \|\mathbf{z}\|_1 \text{ subject to } \mathbf{Gz} = \mathbf{d}, \quad (2.7)$$

where $\|\cdot\|_1$ is the ℓ_1 norm, is known to give the exact solution \mathbf{x} of (2.2) under various conditions satisfied by \mathbf{G} and \mathbf{x} , like the null space property [18], the restricted isometry property [10], conditions based on the mutual coherence [24] and the cumulative coherence [36]. Relaxations of (2.6) of the form

$$\mathcal{P}_{1,q}: \text{ minimize } \|\mathbf{Z}\|_{1,q} \text{ subject to } \mathbf{GZ} = \mathbf{D}, \quad \text{where } \|\mathbf{Z}\|_{1,q} = \sum_{j=1}^{N_y} \|\mathbf{z}_{j \rightarrow}\|_q, \quad (2.8)$$

are studied in [19, 31, 15, 27, 38, 37, 39]. Conditions of recoverability of \mathbf{X} by the minimizer of (2.8) are established in [15, Theorem 3.1] and [38, Theorem 5.1]. However, there are no conclusive results that demonstrate the advantage of the MMV formulation over the SMV one in the convex relaxation form, as discussed for example in [15, Section D], [38, Section 5.2] and [39, Section 3.2].

These studies make no assumption on the structure of the unknown \mathbf{X} , except for sparsity of its row support \mathcal{S} , and do not address the case of more general imaging scenes where exact reconstructions of \mathbf{X} may not be achieved. Our resolution theory quantifies the error of the reconstruction based on the separation between the points in $\Omega_{\mathcal{S}}$, the correlation of the rows of \mathbf{X} and the noise level. We show in particular that if \mathbf{X} has uncorrelated rows, the MMV formulation may have an advantage over SMV. This is relevant to SAR imaging, as explained in section 3.

2.2. Resolution theory. Let us consider the following modification of the linear system (2.1)

$$\mathbf{D}_{\mathbf{W}} = \mathbf{GX} + \mathbf{W}, \quad (2.9)$$

which accounts for data $\mathbf{D}_{\mathbf{W}} \in \mathbb{C}^{N_r \times N_v}$ contaminated by the noise matrix $\mathbf{W} \in \mathbb{C}^{N_r \times N_v}$. We estimate \mathbf{X} by the minimizer \mathbf{X}^ε of the convex problem

$$\mathcal{P}_{1,2}^\varepsilon: \text{ minimize } \|\mathbf{Z}\|_{1,2} \text{ subject to } \|\mathbf{GZ} - \mathbf{D}_{\mathbf{W}}\|_F \leq \varepsilon, \quad (2.10)$$

where $\|\cdot\|_F$ is the Frobenius norm and ε is a chosen tolerance, satisfying

$$\|\mathbf{W}\|_F < \varepsilon. \quad (2.11)$$

Our goal is to quantify the approximation of \mathbf{X} by \mathbf{X}^ε , by taking into account the separation of the points in $\Omega_{\mathcal{S}}$ and the correlation of the rows of \mathbf{X} . These determine how the unknowns interact with each other, as described by the \mathbf{X} dependent "multiple view interaction coefficient" \mathcal{I}_{N_v} defined in section 2.2.1. The smaller \mathcal{I}_{N_v} is, the better the imaging results, as stated by the estimates in sections 2.2.2–2.2.4. We also study in section 2.2.5 the case of clusters of points in $\Omega_{\mathcal{S}}$, where \mathcal{I}_{N_v} is large and the previous estimates are not useful. We introduce a new interaction coefficient for the cluster, which is much smaller than \mathcal{I}_{N_v} , and show that when this is small, the MMV reconstruction is supported in the vicinity of $\Omega_{\mathcal{S}}$.

2.2.1. The multiple view interaction coefficient. The interaction between the unknowns is quantified by the \mathbf{X} dependent multiple view interaction coefficient defined by

$$\mathcal{I}_{N_v} = \max_{1 \leq j \leq N_{\mathbf{y}}} \sup_{\mathbf{v}_{\rightarrow} \in \mathbb{C}^{1 \times N_v}} \sum_{q \in \mathcal{S} \setminus \{n(j)\}} |\mu(\mathbf{g}_j, \mathbf{g}_q)| |\mu(\mathbf{v}_{\rightarrow}, \mathbf{x}_{q\rightarrow})|, \quad (2.12)$$

using the correlation of the columns of \mathbf{G} ,

$$\mu(\mathbf{g}_j, \mathbf{g}_q) = \langle \mathbf{g}_j, \mathbf{g}_q \rangle, \quad 1 \leq j, q \leq N_{\mathbf{y}}, \quad (2.13)$$

where $\langle \mathbf{g}_j, \mathbf{g}_q \rangle = \mathbf{g}_j^* \mathbf{g}_q$ is the Hermitian inner product, and \star denotes complex conjugate and transpose. These columns are normalized, so that

$$\|\mathbf{g}_j\|_2 = \langle \mathbf{g}_j, \mathbf{g}_j \rangle^{1/2} = 1, \quad 1 \leq j \leq N_{\mathbf{y}}, \quad (2.14)$$

and we suppose that

$$|\mu(\mathbf{g}_j, \mathbf{g}_q)| < 1, \quad \forall j \neq q, \quad 1 \leq j, q \leq N_{\mathbf{y}}. \quad (2.15)$$

This assumption holds in the SAR imaging application and it allows us to quantify the distance between the points using the semimetric

$$\mathfrak{D} : \{1, \dots, N_{\mathbf{y}}\} \times \{1, \dots, N_{\mathbf{y}}\} \rightarrow [0, 1], \quad \mathfrak{D}(j, q) = 1 - |\mu(\mathbf{g}_j, \mathbf{g}_q)|. \quad (2.16)$$

We will see in section 3 that $|\mu(\mathbf{g}_j, \mathbf{g}_q)|$ is approximately a function of $\mathbf{y}_j - \mathbf{y}_q$, which peaks at the origin i.e., for $\mathbf{y}_j = \mathbf{y}_q$, and decreases monotonically in the vicinity of the peak. Thus, points at small distance with respect to \mathfrak{D} are also close in the Euclidian distance.

We use the semimetric \mathfrak{D} in definition (2.12) to select the closest point to \mathbf{y}_j in $\Omega_{\mathcal{S}}$, indexed by $n(j) \in \mathcal{S}$. If this point is not unique, we just pick one and let $n(j)$ be its index. In an abuse of notation, we also let $\mu(\cdot, \cdot)$ be the correlation of the rows of \mathbf{X} with \mathbf{v}_{\rightarrow} , defined by

$$\mu(\mathbf{v}_{\rightarrow}, \mathbf{x}_{q\rightarrow}) = \frac{\langle \mathbf{v}_{\rightarrow}, \mathbf{x}_{q\rightarrow} \rangle}{\|\mathbf{v}_{\rightarrow}\|_2 \|\mathbf{x}_{q\rightarrow}\|_2}, \quad (2.17)$$

where $\langle \mathbf{v}_{\rightarrow}, \mathbf{x}_{q\rightarrow} \rangle = \mathbf{v}_{\rightarrow} \mathbf{x}_{q\rightarrow}^*$ is the Hermitian inner product of row vectors and $\|\cdot\|_2$ is the induced ℓ_2 norm.

Note that (2.17) has absolute value equal to 1 in the SMV setting, where $N_v = 1$ and \mathbf{v}_{\rightarrow} and $\mathbf{x}_{k\rightarrow}$ are complex numbers. Then, (2.12) reduces to the single view interaction coefficient \mathcal{I}_1 used in [7, Section 4] to quantify the quality of imaging with ℓ_1 optimization. As shown in [7], \mathcal{I}_1 is small if the points in $\Omega_{\mathcal{S}}$ are sufficiently far apart. Here we consider $N_v > 1$, and note that since $|\mu(\mathbf{v}_{\rightarrow}, \mathbf{x}_{k\rightarrow})| \leq 1$, we have $\mathcal{I}_{N_v} \leq \mathcal{I}_1$. In section 2.2.4 we show that depending on the correlation of the rows of \mathbf{X} , we may have $\mathcal{I}_{N_v} \ll \mathcal{I}_1$. The resolution estimates below show an advantage of using MMV in such cases.

2.2.2. Estimation of the support of \mathbf{X} . The next theorem, proved in section 5.2, shows that when \mathcal{I}_{N_v} and the noise level ε are small, the large entries in \mathbf{X}^ε are supported at points near $\Omega_{\mathcal{S}}$.

THEOREM 2.1. *Consider the matrix $\mathbf{W}^\varepsilon = \mathbf{G}(\mathbf{X}^\varepsilon - \mathbf{X})$, defined in terms of the unknown \mathbf{X} and its reconstruction \mathbf{X}^ε , the minimizer of (2.10). This matrix cannot be computed but it is guaranteed to satisfy*

$$\|\mathbf{W}^\varepsilon\|_F \leq 2\varepsilon. \quad (2.18)$$

Suppose that there exists $r \in (0, 1)$ so that $2\mathcal{I}_{N_v} < r < 1$, and define the set

$$\mathfrak{B}_r(\mathcal{S}) = \{1 \leq j \leq N_{\mathbf{y}} \text{ such that } \exists q \in \mathcal{S} \text{ satisfying } \mathfrak{D}(j, q) < r\},$$

called the r -vicinity of \mathcal{S} with respect to the semimetric \mathfrak{D} . If we decompose the reconstruction in two parts

$$\mathbf{X}^\varepsilon = \mathbf{X}^{\varepsilon, r} + \mathbf{E}^{\varepsilon, r}, \quad (2.19)$$

with $\mathbf{X}^{\varepsilon,r}$ row supported in $\mathfrak{B}_r(\mathcal{S})$ and $\mathbf{E}^{\varepsilon,r}$ row supported in the complement $\{1, \dots, N_{\mathbf{y}}\} \setminus \mathfrak{B}_r(\mathcal{S})$, we have

$$\|\mathbf{E}^{\varepsilon,r}\|_{1,2} \leq \frac{2\mathcal{I}_{N_v}}{r} \|\mathbf{X}^\varepsilon\|_{1,2} + \frac{1}{r} \|(\mathbf{G}^* \mathbf{W}^\varepsilon)_{\mathcal{S} \rightarrow}\|_{1,2} \leq \frac{2\mathcal{I}_{N_v}}{r} \|\mathbf{X}^\varepsilon\|_{1,2} + \frac{2\varepsilon|\mathcal{S}|}{r}, \quad (2.20)$$

where $\mathbf{G}^* \in \mathbb{C}^{N_{\mathbf{y}} \times N_r}$ is the Hermitian adjoint of \mathbf{G} and $(\mathbf{G}^* \mathbf{W}^\varepsilon)_{\mathcal{S} \rightarrow} \in \mathbb{C}^{|\mathcal{S}| \times N_v}$ is the restriction of the matrix $\mathbf{G}^* \mathbf{W}^\varepsilon$ to the rows indexed by the entries in \mathcal{S} .

We may think of $\mathbf{E}^{\varepsilon,r}$ as an error in the reconstruction, because its rows are supported away from \mathcal{S} . The theorem says that this error is small when the multiple interaction coefficient and the noise level are small. The estimate of the noise effect in the second bound in (2.20) is pessimistic. In the numerical simulations we found that $\|(\mathbf{G}^* \mathbf{W}^\varepsilon)_{\mathcal{S} \rightarrow}\|_{1,2}$ is typically much smaller than $2\varepsilon|\mathcal{S}|$.

2.2.3. Quantitative estimation of \mathbf{X} . Theorem 2.1 says that if we threshold the entries in \mathbf{X}^ε at a value commensurate to the right hand side in (2.20), we obtain the approximation $\mathbf{X}^{\varepsilon,r}$ with row support $\mathcal{S}^\varepsilon \subset \mathfrak{B}_r(\mathcal{S})$. Here we quantify how well $\mathbf{X}^{\varepsilon,r}$ approximates \mathbf{X} . Because \mathcal{S} and \mathcal{S}^ε are different sets in general, an estimate of some norm of $\mathbf{X}^{\varepsilon,r} - \mathbf{X}$ is not useful. Instead, we decompose $\mathbf{X}^{\varepsilon,r}$ in one part supported in \mathcal{S} that we compare with \mathbf{X} in Theorem 2.2, and a residual.

Let $\mathbf{G}_{\mathcal{S}} = (\mathbf{g}_j)_{j \in \mathcal{S}}$ be the $N_r \times |\mathcal{S}|$ matrix obtained by restricting the columns of \mathbf{G} to the indexes in \mathcal{S} . Suppose that $\mathbf{G}_{\mathcal{S}}$ has linearly independent columns, as otherwise it is impossible to recover \mathbf{X} even with noiseless data, and introduce its pseudoinverse

$$\mathbf{G}_{\mathcal{S}}^\dagger = (\mathbf{G}_{\mathcal{S}}^* \mathbf{G}_{\mathcal{S}})^{-1} \mathbf{G}_{\mathcal{S}}^*. \quad (2.21)$$

Decompose $\mathbf{X}^{\varepsilon,r}$ in two parts

$$\mathbf{X}^{\varepsilon,r} = \mathfrak{X}^{\varepsilon,r} + \mathcal{E}^{\varepsilon,r}, \quad (2.22)$$

where $\mathfrak{X}^{\varepsilon,r}$ has row support in \mathcal{S} and its restriction to the rows indexed by \mathcal{S} satisfies

$$\mathfrak{X}_{\mathcal{S} \rightarrow}^{\varepsilon,r} = \mathbf{G}_{\mathcal{S}}^\dagger \mathbf{G} \mathbf{X}^{\varepsilon,r}. \quad (2.23)$$

This definition gives that

$$\mathbf{G}_{\mathcal{S}}^\dagger \mathbf{G} \mathbf{X}^{\varepsilon,r} = (\mathbf{G}_{\mathcal{S}}^* \mathbf{G}_{\mathcal{S}})^{-1} \mathbf{G}_{\mathcal{S}}^* (\mathbf{G}_{\mathcal{S}} \mathfrak{X}_{\mathcal{S} \rightarrow}^{\varepsilon,r} + \mathbf{G} \mathcal{E}^{\varepsilon,r}) = \mathfrak{X}_{\mathcal{S} \rightarrow}^{\varepsilon,r} + (\mathbf{G}_{\mathcal{S}}^* \mathbf{G}_{\mathcal{S}})^{-1} \mathbf{G}_{\mathcal{S}}^* \mathbf{G} \mathcal{E}^{\varepsilon,r}, \quad (2.24)$$

so the residual $\mathcal{E}^{\varepsilon,r}$ satisfies

$$\mathbf{G}_{\mathcal{S}}^* \mathbf{G} \mathcal{E}^{\varepsilon,r} = 0. \quad (2.25)$$

That is to say, the columns of $\mathbf{G} \mathcal{E}^{\varepsilon,r}$ are orthogonal to the range of $\mathbf{G}_{\mathcal{S}}$. Note that $\mathcal{E}^{\varepsilon,r}$ has row support in $\mathcal{S} \cup \mathcal{S}^\varepsilon$. If \mathcal{S}^ε were the same as \mathcal{S} , then (2.25) would imply that $\mathcal{E}^{\varepsilon,r} = 0$. Thus, $\mathcal{E}^{\varepsilon,r}$ is a residual that accounts for $\mathbf{X}^{\varepsilon,r}$ not having the exact support \mathcal{S} .

The next theorem, proved in section 5.3, shows that under the same conditions as in Theorem 2.1, the matrix $\mathfrak{X}^{\varepsilon,r}$ is a good approximation of the unknown \mathbf{X} . However, $\mathfrak{X}^{\varepsilon,r}$ cannot be computed directly, so we need to relate it to $\mathbf{X}^{\varepsilon,r}$. To do so, we introduce an ‘‘effective matrix’’ supported in \mathcal{S} , obtained by local aggregation of the rows of $\mathbf{X}^{\varepsilon,r}$. We show that $\mathfrak{X}^{\varepsilon,r}$ is close to this matrix if the single view interaction coefficient \mathcal{I}_1 is small. This reveals the fact that while $\mathcal{I}_{N_v} \ll \mathcal{I}_1$ brings an improved support of the MMV reconstruction vs. that of SMV, the quantitative estimate of \mathbf{X} cannot be expected to be better.

THEOREM 2.2. *Let $\mathbf{X}^{\varepsilon,r}$ and $\mathfrak{X}^{\varepsilon,r}$ be defined as in (2.19) and (2.22). Then,*

$$\|\mathfrak{X}^{\varepsilon,r} - \mathbf{X}\|_{1,2} \leq \frac{2\mathcal{I}_{N_v}}{r} \|\mathbf{X}^\varepsilon\|_{1,2} + \frac{6\varepsilon|\mathcal{S}|}{r}. \quad (2.26)$$

Moreover, if the support of $\mathbf{X}^{\varepsilon,r}$ is decomposed in $|\mathcal{S}|$ disjoint parts, each corresponding to a point in \mathcal{S} ,

$$\mathcal{S}^\varepsilon = \bigcup_{j \in \mathcal{S}} \mathcal{S}_j^\varepsilon, \quad \mathcal{S}_j^\varepsilon = \{q \in \mathcal{S}^\varepsilon \text{ such that } \mathfrak{D}(q, j) \leq \mathfrak{D}(q, j'), \forall j' \in \mathcal{S}\}, \quad j \in \mathcal{S}, \quad (2.27)$$

and we define the effective matrix $\overline{\mathbf{X}}^{\varepsilon,r}$ with row support in \mathcal{S} and entries

$$\overline{\mathbf{X}}_{j,v}^{\varepsilon,r} = \begin{cases} \sum_{l \in \mathcal{S}_j^\varepsilon} \mu(\mathbf{g}_j, \mathbf{g}_l) \mathbf{X}_{l,v}^{\varepsilon,r}, & \text{if } j \in \mathcal{S}, \\ 0, & \text{otherwise,} \end{cases} \quad \text{for } 1 \leq j \leq N_{\mathbf{y}}, 1 \leq v \leq N_v, \quad (2.28)$$

we have the estimate

$$(1 - \mathcal{I}_1) \|\mathbf{x}^{\varepsilon,r} - \overline{\mathbf{X}}^{\varepsilon,r}\|_{1,1} \leq 2\mathcal{I}_1 \|\mathbf{X}^{\varepsilon,r}\|_{1,1}. \quad (2.29)$$

Note that because $\mu(\mathbf{g}_j, \mathbf{g}_l)$ are complex valued, there may be cancellations in the local aggregation (2.28) of the entries of $\mathbf{X}^{\varepsilon,r}$. Only if the set $\mathcal{S}_j^\varepsilon$ is small, so that $\mathfrak{D}(j, l) \ll 1$ for $l \in \mathcal{S}_j^\varepsilon$, we have $\mu(\mathbf{g}_j, \mathbf{g}_l) \approx 1$ and (2.28) is approximately the local sum of the entries in $\mathbf{X}^{\varepsilon,r}$.

2.2.4. Matrices \mathbf{X} with orthogonal rows. We now show that if the unknown matrix \mathbf{X} has orthogonal rows[†] (i.e., uncorrelated), then the multiple view interaction coefficient \mathcal{I}_{N_v} may be much smaller than the interaction coefficient \mathcal{I}_1 . By Theorem 2.1, this means that the MMV approach can give improved estimates of the row support \mathcal{S} of \mathbf{X} , under less stringent conditions than in the SMV formulation.

PROPOSITION 2.3. *Suppose that $\mathbf{X} \in \mathbb{C}^{N_{\mathbf{y}} \times N_v}$ has row support in the set \mathcal{S} with cardinality $1 < |\mathcal{S}| \leq N_v$, and that its nonzero rows are orthogonal. Then, the multiple view interaction coefficient (2.12) is given by*

$$\mathcal{I}_{N_v} = \max_{1 \leq j \leq N_{\mathbf{y}}} \sqrt{\sum_{q \in \mathcal{S} \setminus \{n(j)\}} |\mu(\mathbf{g}_j, \mathbf{g}_q)|^2}. \quad (2.30)$$

This proposition, proved in section 5.4, gives a simpler expression of \mathcal{I}_{N_v} , that we can compare with

$$\mathcal{I}_1 = \max_{1 \leq j \leq N_{\mathbf{y}}} \sum_{q \in \mathcal{S} \setminus \{n(j)\}} |\mu(\mathbf{g}_j, \mathbf{g}_q)|, \quad (2.31)$$

to understand when $\mathcal{I}_{N_v} \ll \mathcal{I}_1$. For this purpose, let us define the vector $\boldsymbol{\gamma}^{(j)} \in \mathbb{R}^{1 \times (|\mathcal{S}|-1)}$ with entries $|\mu(\mathbf{g}_j, \mathbf{g}_q)|$, for $q \in \mathcal{S} \setminus \{n(j)\}$, and rewrite (2.30) and (2.31) as

$$\mathcal{I}_{N_v} = \max_{1 \leq j \leq N_{\mathbf{y}}} \|\boldsymbol{\gamma}^{(j)}\|_2, \quad \mathcal{I}_1 = \max_{1 \leq j \leq N_{\mathbf{y}}} \|\boldsymbol{\gamma}^{(j)}\|_1, \quad (2.32)$$

using the ℓ_2 and ℓ_1 vector norms. Suppose that the maximizer in the definition of \mathcal{I}_{N_v} is at index $j = m$. Basic vector norm inequalities give the general relation

$$\mathcal{I}_{N_v} = \|\boldsymbol{\gamma}^{(m)}\|_2 \leq \|\boldsymbol{\gamma}^{(m)}\|_1 \leq \mathcal{I}_1,$$

which is nothing new than was discussed previously. However, if we assume further that the entries in $\boldsymbol{\gamma}^{(m)}$ are of the same order, meaning that there exist positive numbers β^- and β^+ , ordered as $\beta^- \leq \beta^+$ and satisfying $\beta^+/\beta^- = O(1)$, such that

$$\beta^- \leq |\mu(\mathbf{g}_m, \mathbf{g}_q)| \leq \beta^+, \quad \forall q \in \mathcal{S} \setminus \{n(m)\}, \quad (2.33)$$

then we have

$$\mathcal{I}_{N_v} \leq \beta^+ \sqrt{|\mathcal{S}| - 1} = \frac{\beta^+ [\beta^- (|\mathcal{S}| - 1)]}{\beta^- \sqrt{|\mathcal{S}| - 1}} \leq \frac{\beta^+ \|\boldsymbol{\gamma}^{(m)}\|_1}{\beta^- \sqrt{|\mathcal{S}| - 1}} \leq \frac{\beta^+ \mathcal{I}_1}{\beta^- \sqrt{|\mathcal{S}| - 1}} = O\left(\frac{\mathcal{I}_1}{\sqrt{|\mathcal{S}| - 1}}\right). \quad (2.34)$$

Recalling the discussion below definition (2.16) of the semimetric \mathfrak{D} and that $|\mu(\mathbf{g}_m, \mathbf{g}_q)| = 1 - \mathfrak{D}(m, q)$, we can interpret (2.33) as having points in $\Omega_{\mathcal{S}}$ evenly distributed, at similar spacing. If this condition holds, then \mathcal{I}_{N_v} is smaller than \mathcal{I}_1 , by order $\sqrt{|\mathcal{S}|}$. In practice, it may be difficult to have a large number $|\mathcal{S}|$ of points at similar distance in the imaging plane, in order to see the improvement predicted by (2.34). However, this is just a bound, and the numerical simulations in section 3.4.1 show that a significant reduction of $\mathcal{I}_{N_v}/\mathcal{I}_1$ is achieved even when the imaging region is reduced to a line.

[†]The results extend to nearly orthogonal rows, but to simplify the proof we assume orthogonality.

2.2.5. Clusters of unknowns. The multiple view interaction coefficient \mathcal{J}_{N_v} may be large for arbitrary distributions of points in Ω_S , so we cannot conclude from the estimates above that the reconstruction \mathbf{X}^ε approximates \mathbf{X} . However, if the points are clustered around a few locations, indexed by the elements in the set $\mathcal{C} \subset \{1, \dots, N_y\}$ of cardinality $|\mathcal{C}| \ll |\mathcal{S}|$, the reconstruction is still useful, as we now show.

The result follows by recasting Theorem 2.1 for the new linear system

$$\mathbf{G}\mathbf{U} + \mathbf{W} = \mathbf{D}_W, \quad (2.35)$$

with cluster unknown matrix \mathbf{U} and redefined "noise" $\mathbf{W} = \mathbf{W} + \mathbf{G}\mathbf{R}$, with $\mathbf{R} = \mathbf{X} - \mathbf{U}$. The matrix \mathbf{U} is defined by projection of \mathbf{X} on the set of matrices with row support in \mathcal{C} , such that its restriction to the rows indexed by \mathcal{C} satisfies

$$\mathbf{U}_{\mathcal{C} \rightarrow} = \mathbf{G}_{\mathcal{C}}^\dagger \mathbf{G}\mathbf{X}. \quad (2.36)$$

Here $\mathbf{G}_{\mathcal{C}}^\dagger$ is the pseudoinverse of $\mathbf{G}_{\mathcal{C}} = (\mathbf{g}_j)_{j \in \mathcal{C}}$, the restriction of the sensing matrix to the columns indexed in \mathcal{C} , assumed to have full column rank. A similar calculation to that in (2.24) implies that the "residual" \mathbf{R} satisfies $\mathbf{G}_{\mathcal{C}}^\dagger \mathbf{G}\mathbf{R} = 0$, meaning that the columns of $\mathbf{G}\mathbf{R}$ are orthogonal to the range of $\mathbf{G}_{\mathcal{C}}$. In other words, \mathbf{R} accounts for the row support \mathcal{S} of \mathbf{X} being different from \mathcal{C} . The magnitude of this residual depends on how close the points are clustered together, as stated in the next lemma proved in section 5.5.

LEMMA 2.4. *Decompose the set \mathcal{S} in $|\mathcal{C}|$ disjoint parts, called "cluster sets", indexed by the entries in \mathcal{C} ,*

$$\mathcal{S} = \bigcup_{j \in \mathcal{C}} \mathcal{S}_j, \quad \mathcal{S}_j = \{q \in \mathcal{S} \text{ such that } \mathfrak{D}(q, j) < \mathfrak{D}(q, j'), \forall j' \in \mathcal{C}, j' \neq j\}, \quad j \in \mathcal{C}. \quad (2.37)$$

Suppose that each cluster set \mathcal{S}_j is supported within a ball of radius r_c around the point $j \in \mathcal{C}$, with respect to the semimetric \mathfrak{D} , for all $j \in \mathcal{C}$, and that $\mathfrak{D}(j, j') > r_c$ for all distinct $j', j \in \mathcal{C}$. Then,

$$\|\mathbf{G}\mathbf{R}\|_F \leq \sqrt{2r_c} \|\mathbf{X}^T\|_{2,1}, \quad (2.38)$$

where the index T denotes the transpose.

The next theorem, proved in section 5.5, is the extension of Theorem 2.1. It says that if the cluster radius r_c and the cluster multiple view interaction coefficient

$$\mathcal{J}_{N_v}^U = \max_{1 \leq j \leq N_y} \sup_{\mathbf{v}_{\rightarrow} \in \mathbb{C}^{1 \times N_v}} \sum_{q \in \mathcal{C} \setminus \{n(j)\}} |\mu(\mathbf{g}_j, \mathbf{g}_q)| |\mu(\mathbf{v}_{\rightarrow}, \mathbf{u}_{q \rightarrow})| \quad (2.39)$$

are small, the MMV reconstruction is row supported near \mathcal{C} . This is an improvement over the estimate in Theorem 2.1, because $\mathcal{J}_{N_v}^U$ is much smaller than \mathcal{J}_{N_v} when the points in \mathcal{C} are well separated.

THEOREM 2.5. *Let \mathbf{X}^ε be the minimizer of (2.10), with ε chosen large enough to satisfy*

$$\|\mathbf{W}\|_F = \|\mathbf{W} + \mathbf{G}\mathbf{R}\|_F < \varepsilon. \quad (2.40)$$

Decompose \mathbf{X}^ε it in two parts

$$\mathbf{X}^\varepsilon = \mathbf{U}^{\varepsilon, r} + \mathbf{E}^{\varepsilon, r}, \quad (2.41)$$

where $\mathbf{U}^{\varepsilon, r}$ is row supported in the set $\mathfrak{B}_r(\mathcal{C})$, the r vicinity of \mathcal{C} with respect to the semimetric \mathfrak{D} , and $\mathbf{E}^{\varepsilon, r}$ is the error supported in the complement $\{1, \dots, N_y\} \setminus \mathfrak{B}_r(\mathcal{C})$. This satisfies the estimate

$$\|\mathbf{E}^{\varepsilon, r}\|_{1,2} \leq \frac{2\mathcal{J}_{N_v}^U}{r} \|\mathbf{X}^\varepsilon\|_{1,2} + \frac{1}{r} \|(\mathbf{G}^* \mathbf{W}^\varepsilon)_{\mathcal{C} \rightarrow}\|_{1,2}, \quad (2.42)$$

with $\mathbf{W}^\varepsilon = \mathbf{G}(\mathbf{X}^\varepsilon - \mathbf{X})$ defined as in Theorem 2.1.

An extension of the quantitative estimate in Theorem 2.2 is possible, but we omit it here for brevity. The result says that we should expect a good qualitative agreement between \mathbf{X}^ε and a local aggregate of \mathbf{X} over the cluster sets, if the single view interaction coefficient \mathcal{J}_1^U is small, meaning that the points in \mathcal{C} are sufficiently far apart.

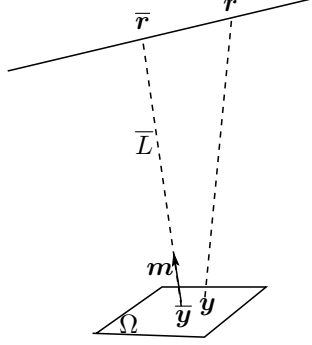


FIG. 3.1. Setup for SAR imaging using a linear synthetic aperture centered at $\bar{\mathbf{r}}$, at distance \bar{L} from the center $\bar{\mathbf{y}}$ of the imaging region Ω . The antenna locations \mathbf{r} span the aperture of length a , and \mathbf{y} denotes a point in Ω . The unit vector $\mathbf{m} = (\bar{\mathbf{r}} - \bar{\mathbf{y}})/\bar{L}$ pointing from $\bar{\mathbf{y}}$ to $\bar{\mathbf{r}}$ defines the range direction.

3. SAR imaging of direction dependent reflectivity. In this section we consider the application of SAR imaging of direction dependent reflectivities. We begin with the data model in section 3.1, and then derive in section 3.2 the linear system (2.1). The discussion in these two sections is similar to that in [8], so we keep it short and give only the information that is needed to connect to the theory in section 2.2. We explore in section 3.3 the condition of orthogonality of the rows of \mathbf{X} , assumed in Proposition 2.3, and use numerical simulations in section 3.4 to illustrate the theoretical results.

3.1. The SAR data model. Consider the set-up illustrated in Figure 3.1, where we display a piece of the synthetic aperture spanned by the moving transmit-receive antenna, called a sub-aperture. We approximate the sub-aperture by a line segment along the unit vector $\boldsymbol{\tau}$, with center at location $\bar{\mathbf{r}}$, and length a . The imaging region Ω lies on a plane surface, and is centered at location $\bar{\mathbf{y}}$, at distance $\bar{L} = |\bar{\mathbf{r}} - \bar{\mathbf{y}}|$ from the aperture center $\bar{\mathbf{r}}$. The antenna emits periodically the signal $f(t)$ and measures the back-scattered waves. The waves propagate much faster than the antenna, so we assume that the emission and reception occur at the same location. The antenna moves by a small increment $\Delta\mathbf{r} = \frac{a}{(N_r-1)}\boldsymbol{\tau}$ between two emissions, so the measurements are at locations $\mathbf{r}_j = \bar{\mathbf{r}} - \frac{a\boldsymbol{\tau}}{2} + (j-1)\Delta\mathbf{r}$, for $j = 1, \dots, N_r$.

In the single scattering (Born) approximation, and neglecting for now polarization effects, the scattered wave at \mathbf{r}_j is given by

$$p(\mathbf{r}_j, t; \bar{\mathbf{r}}, \bar{\omega}) = \int \frac{d\omega}{2\pi} e^{-i\omega t} \hat{f}(\omega) k^2(\omega) \sum_{q=1}^{N_y} \rho_q(\bar{\mathbf{r}}, \bar{\omega}) \frac{\exp[2ik(\omega)|\mathbf{r}_j - \mathbf{y}_q]}{(4\pi|\mathbf{r}_j - \mathbf{y}_q|)^2}. \quad (3.1)$$

Here the hat denotes Fourier transform with respect to time, ω is the frequency and $\rho_q(\bar{\mathbf{r}}, \bar{\omega})$ is the reflectivity[‡] of the scatterer at $\mathbf{y}_q \in \Omega$. This depends on the sub-aperture center $\bar{\mathbf{r}}$ and the central frequency $\bar{\omega}$ of the signal f . The integral over ω is over the support $|\omega - \bar{\omega}| \lesssim b$ of \hat{f} , where b is the bandwidth. The propagation of the waves between the antenna location \mathbf{r}_j and \mathbf{y}_q is modeled with the Green's function for Helmholtz's equation in the medium with constant wave speed c , and the wavenumber is $k(\omega) = \omega/c$.

In SAR imaging, the wave-field (3.1) is convolved with the time reversed emitted pulse, delayed by the round trip travel time of the waves between the antenna and the center point $\bar{\mathbf{y}}$ in Ω . This data processing is called down-ramping [20] and we denote the result by

$$d(\mathbf{r}_j, t; \bar{\mathbf{r}}, \bar{\omega}) = p(\mathbf{r}_j, t; \bar{\mathbf{r}}, \bar{\omega}) \star_t f^*(-t - 2|\mathbf{r}_j - \bar{\mathbf{y}}|/c), \quad (3.2)$$

where f^* denotes the complex conjugate of f . The convolution $f(t) \star_t f^*(-t)$ is called the pulse compressed signal. We denote it by $\varphi(bt) = f(t) \star_t f^*(-t)$, with function φ of dimensionless argument. This is supported at $t = O(1/b)$.

[‡]The reflectivity is assumed slowly changing so it can be approximated by a constant over this sub-aperture and bandwidth.

Let us define the unit vector $\mathbf{m} = (\bar{\mathbf{r}} - \bar{\mathbf{y}})/\bar{L}$ which determines the so-called range direction in imaging, and the orthogonal projection $\mathbb{P} = \mathbf{I} - \mathbf{m}\mathbf{m}^T$ in the cross-range plane, orthogonal to \mathbf{m} . The size of the imaging region in the range and cross-range direction is given by the length scales

$$Y = \sup_{\mathbf{y} \in \Omega} |(\mathbf{y} - \bar{\mathbf{y}}) \cdot \mathbf{m}|, \quad Y^\perp = \sup_{\mathbf{y} \in \Omega} |\mathbb{P}(\mathbf{y} - \bar{\mathbf{y}})|.$$

We assume a typical imaging regime defined by the scale order $\bar{L} \gg a > Y^\perp \gg \bar{\lambda}$ and Fresnel numbers

$$\frac{a^2}{\lambda \bar{L}} \gtrsim \frac{(Y^\perp)^2}{\lambda \bar{L}} \gtrsim 1, \quad (3.3)$$

where $\bar{\lambda} = 2\pi/\bar{k}$ is the central wavelength and $\bar{k} = k(\bar{\omega}) = \bar{\omega}/c$. These inequalities mean physically that the wave front observed at the sub-aperture or in Ω is not planar. If this were not the case, it would be impossible to localize the scatterers in cross-range.

Since the cross-range resolution of classic SAR imaging [17] equals $\bar{\lambda}\bar{L}/a$, the inequalities (3.3) ensure that Y^\perp is larger than this limit, so image focusing can be observed. The range resolution is determined by the accuracy of travel time estimation from the down-ramped data (3.2). It is of the order c/b , so typically $Y \gtrsim c/b$. In most imaging systems $b \ll \bar{\omega}$. To simplify the data model, we assume a bandwidth and aperture segmentation in small enough sub-bands b and sub-aperture sizes a so that

$$\frac{b}{\bar{\omega}} \frac{aY^\perp}{\lambda \bar{L}} \ll 1, \quad \frac{a^2Y}{\lambda \bar{L}^2} \ll 1, \quad \frac{a^2Y^\perp}{\lambda \bar{L}^2} \ll 1. \quad (3.4)$$

Under these scaling assumptions and using the approximations described in [8, Section 3.1], we can write (3.2) in the form

$$\mathcal{D}_j(\bar{\mathbf{r}}) = \sum_{q=1}^{N_y} \frac{\exp \left[-2i\bar{k} \frac{\Delta \mathbf{r}_j \cdot \mathbb{P} \Delta \mathbf{y}_q}{\bar{L}} \right]}{\sqrt{N_r}} \mathcal{X}_q(\bar{\mathbf{r}}), \quad (3.5)$$

with the notation $\Delta \mathbf{r}_j = \mathbf{r}_j - \bar{\mathbf{r}}$ and $\Delta \mathbf{y}_q = \mathbf{y}_q - \bar{\mathbf{y}}$. Here $\mathcal{D}_j(\bar{\mathbf{r}})$ are the down-ramped data (3.2), up to some scaling factor, and evaluated at a fixed time \bar{t} ,

$$\mathcal{D}_j(\bar{\mathbf{r}}) = d(\mathbf{r}_j, \bar{t}; \bar{\mathbf{r}}, \bar{\omega}) e^{i\bar{k}\bar{t}} \left(\frac{4\pi\bar{L}}{k} \right)^2, \quad (3.6)$$

whereas

$$\mathcal{X}_q(\bar{\mathbf{r}}) = \rho_q(\bar{\mathbf{r}}, \omega) \sqrt{N_r} \varphi \left[b \left(\bar{t} + \frac{2\mathbf{m} \cdot \Delta \mathbf{y}_q}{c} \right) \right] \exp \left[-2i\bar{k} \left(\mathbf{m} \cdot \Delta \mathbf{y}_q - \frac{\Delta \mathbf{y}_q \cdot \mathbb{P} \Delta \mathbf{y}_q}{2\bar{L}} \right) \right]. \quad (3.7)$$

We suppressed all the constant variables in the arguments of \mathcal{D}_j . By fixing the time \bar{t} , we limit the sum in (3.5) to the set of points with range coordinates $\mathbf{m} \cdot \Delta \mathbf{y}_q = -t + O(c/b)$. This set is called a range bin in the SAR literature [20]. We consider a single range bin, and study the estimation in the cross-range direction of the reflectivity, for the single frequency sub-band centered at $\bar{\omega}$.

3.2. The MMV formulation. The multiple views correspond to different sub-apertures of size a , dividing a larger aperture of size A . The sub-apertures are centered at $\bar{\mathbf{r}}_v$, for $v = 1, \dots, N_v$. The noiseless data model for the v -th view is (3.5), with $\bar{\mathbf{r}}$ replaced by $\bar{\mathbf{r}}_v$, \bar{L} replaced by $\bar{L}_v = |\bar{\mathbf{r}}_v - \bar{\mathbf{y}}|$, \mathbf{m} replaced by $\mathbf{m}_v = |\bar{\mathbf{r}}_v - \bar{\mathbf{y}}|/\bar{L}_v$ and \mathbb{P} replaced by $\mathbb{P}_v = \mathbf{I} - \mathbf{m}_v \mathbf{m}_v^T$. We assume for simplicity that the large aperture is linear, along the unit vector $\boldsymbol{\tau}$.

Under technical scaling assumptions described in detail in [8], which mean physically that the imaging points remain within the same classic SAR resolution limits for all the views, we obtain from (3.5) the linear system (2.1), for matrices \mathbf{D} , \mathbf{X} and \mathbf{G} with entries

$$D_{j,v} = \mathcal{D}_j(\bar{\mathbf{r}}_v), \quad X_{q,v} = \mathcal{X}_q(\bar{\mathbf{r}}_j), \quad G_{j,q} = \frac{1}{\sqrt{N_r}} \exp \left[-2i\bar{k} \frac{\Delta \mathbf{r}_j \cdot \mathbb{P}_1 \Delta \mathbf{y}_q}{\bar{L}_1} \right]. \quad (3.8)$$

Note that the sensing matrix \mathbf{G} is defined relative to the first sub-aperture. Its columns \mathbf{g}_q , for $q = 1, \dots, N_{\mathbf{y}}$, have norm one, as assumed in (2.14), and their correlation

$$\mu(\mathbf{g}_q, \mathbf{g}_l) = \sum_{j=1}^{N_r} G_{j,q}^* G_{j,l} = \frac{1}{N_r} \sum_{j=1}^{N_r} \exp \left[-2i\bar{k} \frac{\Delta \mathbf{r}_j \cdot \mathbb{P}_1(\mathbf{y}_q - \mathbf{y}_l)}{\bar{L}_1} \right] \quad (3.9)$$

is a function of $\mathbf{y}_q - \mathbf{y}_l$, as stated below equation (2.16). We can approximate further this correlation by replacing the sum with the integral over the sub-aperture,

$$\mu(\mathbf{g}_q, \mathbf{g}_l) \approx \frac{1}{a} \int_{-a/2}^{a/2} dr \exp \left[-2i\bar{k}r \frac{\boldsymbol{\tau} \cdot \mathbb{P}_1(\mathbf{y}_q - \mathbf{y}_l)}{\bar{L}_1} \right] = \text{sinc} \left[\frac{\bar{k}a\boldsymbol{\tau} \cdot \mathbb{P}_1(\mathbf{y}_q - \mathbf{y}_l)}{\bar{L}_1} \right]. \quad (3.10)$$

This attains its maximum, equal to 1, when $q = l$, and satisfies $|\mu(\mathbf{g}_q, \mathbf{g}_l)| < 1$ for all $q \neq l$, as assumed in (2.15). Moreover, $|\mu(\mathbf{g}_q, \mathbf{g}_l)|$ decays monotonically in the vicinity of its peak, so we can relate the Euclidian distance between the points to the semimetric $\mathfrak{D}(q, l)$, as pointed out below equation (2.16).

3.3. Orthogonality of the rows. To use the results in section 2.2.4, we now study under which conditions the rows $\mathbf{x}_{q \rightarrow}$ of \mathbf{X} are approximately orthogonal. For this purpose, we assume that $\boldsymbol{\rho}_q(\bar{\mathbf{r}}_v, \omega)$ changes slowly with $\bar{\mathbf{r}}_v$, on a length scale larger than a . This is consistent with the MMV formulation, which approximates the reflectivity by a constant for each sub-aperture. We also suppose that the sub-apertures overlap, with two consecutive centers separated by a small distance with respect to a . This allows us to approximate the sums in the correlations of the rows by integrals over the large aperture of linear size A , centered at \mathbf{r}_o .

PROPOSITION 3.1. *There exists a constant $C_{q,l}$ that depends on how fast the reflectivities at points \mathbf{y}_q and \mathbf{y}_l change with direction, such that*

$$|\mu(\mathbf{x}_{q \rightarrow}, \mathbf{x}_{l \rightarrow})| \leq \min\{1, C_{q,l}/|Q|\}, \quad \text{for } q \neq l, \quad q, l = 1, \dots, N_{\mathbf{y}}, \quad Q = 4\pi \frac{A\boldsymbol{\tau} \cdot \mathbb{P}_o(\mathbf{y}_q - \mathbf{y}_l)}{\bar{\lambda}|\mathbf{r}_o - \bar{\mathbf{y}}|}, \quad (3.11)$$

where $\mathbf{m}_o = (\mathbf{r}_o - \bar{\mathbf{y}})/|\mathbf{r}_o - \bar{\mathbf{y}}|$ and $\mathbb{P}_o = \mathbf{I} - \mathbf{m}_o \mathbf{m}_o^T$.

This proposition, proved in Appendix A, shows that the correlation of the rows of the unknown matrix \mathbf{X} is small for points that are separated in cross-range by distances larger than $\bar{\lambda}|\mathbf{r}_o - \bar{\mathbf{y}}|/A$. This length scale is the cross-range resolution of SAR imaging over the large aperture A . It is also the distance at which isotropic scatterers must be separated in order to guarantee unique recovery of their reflectivity with ℓ_1 (SMV) optimization over the large aperture, as follows from [28, 13, 14, 7].

In the linear system (2.1) with matrices (3.8), we use multiple views from sub-apertures of size $a \ll A$. Each single view corresponds to an SMV problem, and the condition of unique recovery for that problem is known to be that the scatterers should be much further apart, at distance of order $\bar{\lambda}|\mathbf{r}_o - \bar{\mathbf{y}}|/a$. In MMV we use the entire large aperture, segmented in N_v smaller sub-apertures.

When the scatterers are approximately isotropic, the constant in (3.11) is $C_{q,l} \approx 2$. In this case there is no need to segment the aperture, so it is natural to ask if the MMV reconstruction is similar to the SMV one, over the large aperture. This is a difficult question, but we can say from the results in section 2.2.4 that MMV will work better[§] than SMV over one sub-aperture, because the rows of the unknown matrix \mathbf{X} are approximately orthogonal when the points in its support are at distances of order $\bar{\lambda}|\mathbf{r}_o - \bar{\mathbf{y}}|/A \ll \bar{\lambda}|\mathbf{r}_o - \bar{\mathbf{y}}|/a$. The numerical simulations in the next section demonstrate that this is the case, as well.

When the scatterers have a stronger dependence on direction, the SMV approach over the large aperture does not work well. Aperture segmentation is needed to avoid systematic modeling errors in the optimization. While we may apply the SMV approach for a single sub-aperture, Proposition 3.1 and the results in section 2.2.4 show that the MMV method performs better.

[§]As shown in section 2.2.4, the improvement is dependent on the distribution of the scatterers in the imaging region.

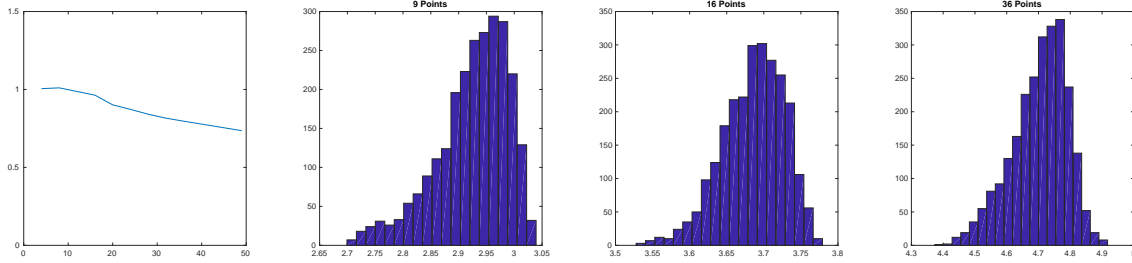


FIG. 3.2. Left plot: The ratio $\frac{\mathcal{I}_1}{\mathcal{I}_{N_v} \sqrt{|S|}}$ vs. $|S|$ in the abscissa. The other plots: Histograms of the ratio $\mathcal{I}_1/\mathcal{I}_{N_v}$ for 2500 realizations of the imaging scene. From left to right $|S|$ equals 9, 16 and 36. The ordinate shows the number of realizations and the abscissa is the value of $\mathcal{I}_1/\mathcal{I}_{N_v}$.

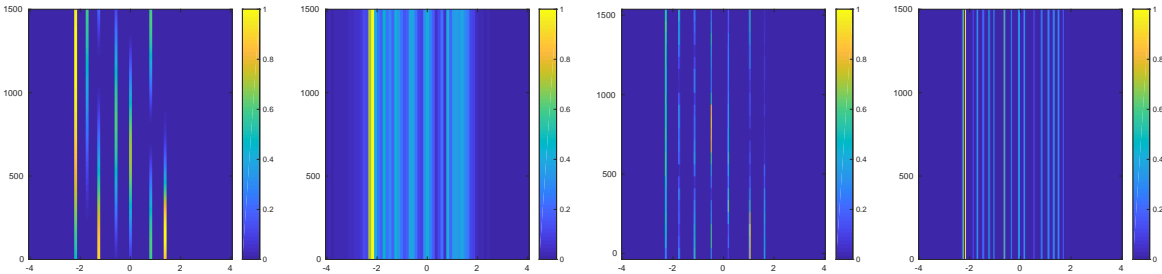


FIG. 3.3. From left to right: (1) Exact reflectivity function as viewed from the location on the flight path (ordinate, in meters) vs. the cross-range location in the imaging scene (abscissa, in units $\lambda \bar{L}_o/A$). (2) The conventional SAR image (3.12) calculated over the entire aperture. (3) The MMV reconstruction. (4) The SMV reconstruction.

3.4. Numerical results. We present here numerical results that illustrate the theory presented in section 2.2. We begin in section 3.4.1 with a computational assessment of the reduction of the multiple view interaction coefficient with respect to the single view one, in the case of orthogonal rows of the unknown matrix \mathbf{X} . Then we present in section 3.4.2 imaging results, using the parameters of the X-band GOTCHA SAR data set [1]: The receive-transmit platform moves on a linear aperture $A = 1.5\text{km}$ at altitude 8km, and with center $\bar{\mathbf{r}}_o$ at 7km west of $\bar{\mathbf{y}}$. The platform emits and receives signals every meter. The central frequency is 10GHz and since we only present imaging in cross-range, the bandwidth plays no role. The waves propagate at speed $c = 3 \cdot 10^8\text{m/s}$.

The data are generated numerically using the single scattering approximation. The additive noise matrix \mathbf{W} has mean zero and independent complex Gaussian entries with standard deviation σ given as a percent of the largest entry in \mathbf{D} . The optimization problem (2.10) is solved using the software package CVX [21].

3.4.1. Numerical illustration of effects of orthogonality of rows of \mathbf{X} . The discussion in section 2.2.4 says that if the points in Ω_S are distributed evenly in the imaging window Ω , and the rows of \mathbf{X} are orthogonal, then the multiple view interaction coefficient \mathcal{I}_{N_v} is smaller than \mathcal{I}_1 , by a factor of order $\sqrt{|S|}$. Here we focus attention on imaging in the cross-range direction, so the imaging region is reduced to a line segment. We cannot have a large number of points with similar mutual separation on a line. Nevertheless, we show that the numerically computed ratio $\mathcal{I}_1/\mathcal{I}_{N_v}$ increases with $|S|$, at a slightly slower rate than $\sqrt{|S|}$.

We display in Figure 3.2 the ratio $\mathcal{I}_1/\mathcal{I}_{N_v}$ computed for imaging scenes with $|S|$ ranging from 4 to 50, and cross-range separation of nearby neighbors chosen randomly, uniformly distributed in the interval $[\lambda \bar{L}_o/A, 3\lambda \bar{L}_o/A]$, where $\bar{L}_o = |\bar{\mathbf{r}}_o - \bar{\mathbf{y}}|$. The large aperture A is divided in sub-apertures of size $a = A/20$. The rows of \mathbf{X} have length 50 and are orthogonal, to stay within the setting of section 2.2.4.

The left plot in Figure 3.2 shows the ratio $\mathcal{I}_1/(\mathcal{I}_{N_v} \sqrt{|S|})$ computed for one realization of the imaging scene. We note that the increase of $\mathcal{I}_1/\mathcal{I}_{N_v}$ with $|S|$ is slightly slower than $\sqrt{|S|}$. The histograms in Figure 3.2, computed for 2500 realizations of the imaging scene, also show that the ratio is slightly less than $\sqrt{|S|}$.

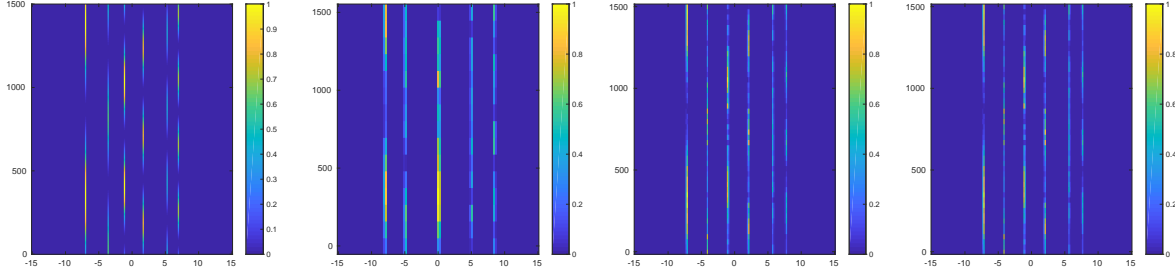


FIG. 3.4. *Left plot: Exact reflectivity function as viewed from the location on the flight path (ordinate, in meters), vs. the cross-range location in the imaging scene (abscissa, in units $\bar{\lambda}\bar{L}_o/A$). Other plots: The MMV reconstruction for apertures $a = 50\text{m}$, 70m and 100m , from left to right.*

3.4.2. Imaging results. We begin with a comparison of imaging results obtained with the MMV optimization formulation (2.10) for $N_v = 24$, the SMV formulation for $N_v = 1$, and the conventional SAR image. The latter is given by the superposition of the down-ramped data (3.2), synchronized using the round-trip travel time of the waves from the radar platform to the imaging point

$$I^{SAR}(\mathbf{y}; \bar{\mathbf{r}}) = \sum_{j=1}^{N_r} d(\mathbf{r}_j, t = 2|\mathbf{r}_j - \mathbf{y}|/c; \bar{\mathbf{r}}, \bar{\omega}). \quad (3.12)$$

The superposition may be over the entire aperture centered at $\bar{\mathbf{r}} = \bar{\mathbf{r}}_o$, in which case $N_r = 1500$, or over a sub-aperture, centered at $\bar{\mathbf{r}} = \bar{\mathbf{r}}_v$ for $v = 1, \dots, N_v$, in which case $N_r = 300$. The sub-aperture length is $a = A/6 = 300\text{m}$, and the spacing between the sub-apertures is 50m , center to center. The results in Figures 3.3–3.4 are for noiseless data and in Figure 3.5 we consider noise with standard deviation $\sigma = 10\%$.

The images in Figure 3.3 are obtained for a scene with 6 small scatterers at cross-range locations spaced by distances of approximately $\bar{\lambda}\bar{L}_o/A$. The exact reflectivity is shown in the left plot. The SAR image (3.12) computed over the entire aperture $A = 1.5\text{km}$ is shown in the second plot. Note that this treats the reflectivity as isotropic (i.e., constant along the ordinate). It does not resolve well the location of the five scatterers that are visible only on about a sixth of A , but it obtains a large peak for the one scatterer with reflectivity that varies less with direction. The MMV image recovers exactly the support of the scatterers, whereas the SMV method has many spurious peaks. This is an illustration of the result in section 2.2.3, which says that MMV may give a better estimate of the support of the scatterers. However, the estimate of the value of the reflectivity is not accurate, unless the scatterers are further apart.

In Figure 3.4 we consider reflectivities that vary more rapidly over directions, and compare the effect of the size of the sub-aperture on the quality of the reconstructions with the MMV approach. The images show that the best reconstruction is for $a = 70\text{m}$, which corresponds roughly with the scale of variation of the true reflectivity in the top plot. For the smaller aperture $a = 40\text{m}$ (left, bottom plot) the reconstructed support is close but not exact, whereas for the larger aperture $a = 100\text{m}$ (right, bottom plot) the image has spurious peaks caused by the systematic error due to the reflectivity varying on a smaller scale than the sub-aperture. Thus, we conclude that in order to image successfully direction dependent reflectivities, it is necessary to have a good estimate of their scale of variation, so that the aperture is properly segmented.

In Figure 3.4 we display the effect of additive noise with standard deviation $\sigma = 10\%$ on the MMV reconstruction of the reflectivity, for sub-aperture size $a = 70\text{m}$. We note that for such noise the support of the reconstruction is basically unchanged and the values of the reflectivity are only slightly different. Naturally, at higher noise levels, the reconstruction will be worse.

4. SAR imaging with polarization diverse measurements. In this section we describe briefly the application of SAR imaging with polarization. We begin in section 4.1 with the derivation of the data model (2.1) used in the MMV formulation and then show numerical results in section 4.2.

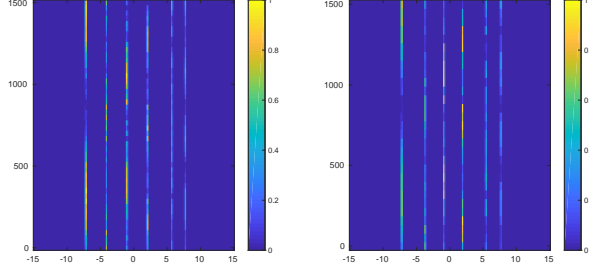


FIG. 3.5. *MMV reconstructions with noiseless data (left) and noisy data (right). The noise is additive, complex Gaussian, with mean zero independent entries and standard deviation $\sigma = 10\%$ of the largest entry in \mathbf{D} . The axes are as in Figure 3.3.*

4.1. Data model. Consider a collection of $|\mathcal{S}|$ penetrable scatterers, with volume smaller than $\bar{\lambda}^3$ by a factor $\alpha \ll 1$, so that the scattered electric field at the SAR platform can be modeled by [3]

$$\mathcal{E}(\mathbf{r}_j, t; \bar{\mathbf{r}}, \mathbf{f}) = \int \frac{d\omega}{2\pi} e^{-i\omega t} i k^3(\omega) \sqrt{\frac{\mu}{\epsilon}} \sum_{q \in \mathcal{S}} \widehat{\mathcal{G}}(\omega, \mathbf{r}_j, \mathbf{y}_q) \boldsymbol{\rho}_q(\bar{\mathbf{r}}) \widehat{\mathcal{G}}(\omega, \mathbf{y}_q, \mathbf{r}_j) \widehat{\mathbf{f}}(\omega) + O(\alpha^4), \quad (4.1)$$

where $\bar{\lambda}$ is the central wavelength and μ and ϵ are the magnetic permeability and the electric permittivity in the medium. These define the wave speed $c = 1/\sqrt{\mu\epsilon}$ and the wavenumber $k(\omega) = \omega/c$. The scatterers are represented in (4.1) by their center location \mathbf{y}_q and their reflectivity tensor assumed constant over the sub-aperture centered at $\bar{\mathbf{r}}$,

$$\boldsymbol{\rho}_q(\bar{\mathbf{r}}) = \alpha^3 \left(\frac{\epsilon_q}{\epsilon} - 1 \right) \mathbf{M}_q(\bar{\mathbf{r}}), \quad (4.2)$$

where ϵ_q is the electric permittivity in the scatterer and \mathbf{M}_q is its α -independent polarization tensor. We refer to [2] for details on \mathbf{M}_q , which depends on the shape of the scatterer. Here we assume that it is a real valued 3×3 symmetric matrix. Since we consider a fixed central frequency $\bar{\omega}$, we suppress in the notation the dependence of $\boldsymbol{\rho}_q$ on $\bar{\omega}$. We also neglect the variation of the magnetic permeability in the scatterer, although this can be taken into account, as shown in [2].

The wave propagation from the radar platform to the scatterers and back is modeled in (4.1) by the dyadic Green's tensor

$$\widehat{\mathcal{G}}(\omega, \mathbf{r}, \mathbf{y}) = \left(\mathbf{I} + \frac{\nabla \nabla^T}{k^2(\omega)} \right) \frac{\exp[ik(\omega)|\mathbf{r} - \mathbf{y}|]}{4\pi|\mathbf{r} - \mathbf{y}|}, \quad (4.3)$$

where \mathbf{I} is the 3×3 identity matrix. The wave excitation is modeled by the vector $\widehat{\mathbf{f}}$. To avoid a lengthy discussion[¶] suppose that the radar emits and receives all possible polarizations, so that we have access to the 3×3 frequency dependent data matrix

$$\widehat{\mathcal{D}}(\mathbf{r}_j, \omega; \bar{\mathbf{r}}) \approx \sum_{q=1}^{N_{\mathbf{y}}} \widehat{\mathcal{G}}(\omega, \mathbf{r}_j, \mathbf{y}_q) \boldsymbol{\rho}_q(\bar{\mathbf{r}}) \widehat{\mathcal{G}}(\omega, \mathbf{y}_q, \mathbf{r}_j), \quad (4.4)$$

with the approximation due to the neglected $O(\alpha^4)$ residual. Here we sum over all the $N_{\mathbf{y}}$ points in the imaging region, with the convention that $\boldsymbol{\rho}_q = 0$ for $q \notin \mathcal{S}$.

As in the previous section, we focus attention on imaging in the cross-range direction. This is why it is sufficient to consider a single frequency, equal to the central one $\bar{\omega}$. The wave number at this frequency is denoted by \bar{k} , as in the previous section.

[¶]In fact, only the transverse components of the electric field, in the plane orthogonal to the range direction $\bar{\mathbf{r}} - \bar{\mathbf{y}}$, play a role in the end, as discussed at the end of this section.

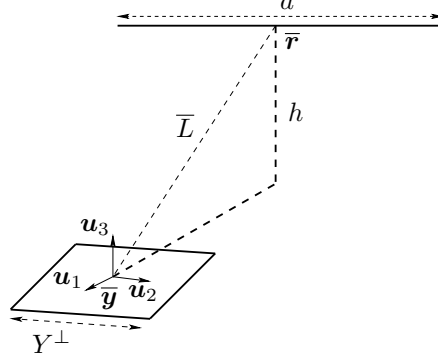


FIG. 4.1. *Geometry of the data acquisition. The radar platform flies at elevation h from the plane surface containing the imaging region Ω , centered at $\bar{\mathbf{y}}$. The distance \bar{L} from the center $\bar{\mathbf{r}}$ of the aperture to $\bar{\mathbf{y}}$ is order h . The drawing is not up to scale, as the aperture a and side Y^\perp of the imaging region are much smaller than \bar{L} .*

The sub-aperture centered at $\bar{\mathbf{r}}$ is linear, of length a , like before, and we assume for simplicity that it is at constant altitude h , as shown in Figure 4.1. We let \mathbf{u}_3 be the unit vector in the vertical direction, and introduce the unit vector $\mathbf{u}_1 = \boldsymbol{\tau} \times \mathbf{u}_3$, where $\boldsymbol{\tau}$ is the unit tangent to the aperture, orthogonal to \mathbf{u}_3 . The imaging region Ω is in the plane spanned by \mathbf{u}_1 and $\boldsymbol{\tau}$. We are interested in its cross-section in the direction of the aperture, which is the cross-range interval centered at $\bar{\mathbf{y}}$, of length Y^\perp .

In the system of coordinates with center at $\bar{\mathbf{y}}$ and orthonormal basis $\{\mathbf{u}_j\}_{1 \leq j \leq 3}$ with $\mathbf{u}_2 = \boldsymbol{\tau}$, we have $\mathbf{r} = r_1 \mathbf{u}_1 + r_2 \mathbf{u}_2 + h \mathbf{u}_3$ and $\mathbf{y} = y_2 \mathbf{u}_2$, for all \mathbf{r} in the aperture and \mathbf{y} in the cross-range imaging interval. We also represent the symmetric 3×3 reflectivity tensor $\boldsymbol{\rho}_q(\bar{\mathbf{r}})$ by the 1×6 row-vector formed with the entries in its upper-tridiagonal part

$$\boldsymbol{\rho}_{q \rightarrow} = (\rho_{q,11}, \rho_{q,22}, \rho_{q,33}, \rho_{q,12}, \rho_{q,13}, \rho_{q,23}), \quad \rho_{q,jl} = \mathbf{u}_j^T \boldsymbol{\rho}_q \mathbf{u}_l.$$

The scaling regime is as in the previous section, with length scales ordered as $\bar{\lambda} \ll Y^\perp \lesssim a \ll h$, satisfying $\bar{L} = |\bar{\mathbf{r}}| = O(h)$ and $|r_j| = O(\bar{L})$, for $j = 1, 2$. The Green tensor (4.3) has the following approximation in this regime

$$\widehat{\mathcal{G}}(\omega, \mathbf{r}_j, \mathbf{y}_q) \approx \frac{\exp[i\bar{k}|\mathbf{r}_j - \mathbf{y}_q|]}{4\pi\bar{L}} \begin{pmatrix} 1 - \eta_1^2 & -\eta_1\eta_2 & -\eta_1\beta \\ -\eta_1\eta_2 & 1 - \eta_2^2 & -\eta_2\beta \\ -\eta_1\beta & -\eta_2\beta & 1 - \beta^2 \end{pmatrix}, \quad \eta_j = \bar{r}_j/\bar{L}, \quad j = 1, 2, \quad \beta = h/\bar{L}. \quad (4.5)$$

Substituting it in (4.4), and representing the symmetric matrix $(4\pi\bar{L})^2/\sqrt{N_r} \widehat{\mathcal{G}}(\mathbf{r}_j, \bar{\omega}; \bar{\mathbf{r}})$ by the 1×6 row vector formed with the entries in its upper triangular part, we obtain the data model

$$\mathbf{d}_{j \rightarrow}(\bar{\mathbf{r}}) = \sum_{q=1}^{N_y} \frac{\exp[2i\bar{k}|\mathbf{r}_j - \mathbf{y}_q|]}{\sqrt{N_r}} \boldsymbol{\rho}_{q \rightarrow}(\bar{\mathbf{r}}) \boldsymbol{\Gamma}(\bar{\mathbf{r}}), \quad j = 1, \dots, N_r, \quad (4.6)$$

with $\bar{\mathbf{r}} = \bar{r}_1 \mathbf{u}_1 + \bar{r}_2 \mathbf{u}_2 + h \mathbf{u}_3$ and constant matrix $\boldsymbol{\Gamma}(\bar{\mathbf{r}})$ given in Appendix B. This is a linear system of form (2.1), for $N_v = 6$, data matrix $\mathbf{D} \in \mathbb{C}^{N_r \times 6}$ with rows $\mathbf{d}_{j \rightarrow}$, unknown matrix $\mathbf{X} \in \mathbb{C}^{N_y \times 6}$ with rows

$$\mathbf{x}_{q \rightarrow} = \boldsymbol{\rho}_{q \rightarrow} \boldsymbol{\Gamma}, \quad (4.7)$$

and sensing matrix \mathbf{G} with normalized columns $\mathbf{g}_q = \frac{1}{\sqrt{N_r}} \left(\exp[2i\bar{k}|\mathbf{r}_1 - \mathbf{y}_q|], \dots, \exp[2i\bar{k}|\mathbf{r}_{N_r} - \mathbf{y}_q|] \right)^T$.

The system (4.6) is for a single sub-aperture. More sub-apertures, centered at $\bar{\mathbf{r}}_v$, can be taken into account as explained in the previous section, with the only difference being that instead of having a scalar unknown, we now have the unknown 1×6 row vector $\boldsymbol{\rho}_q(\bar{\mathbf{r}}_v) \boldsymbol{\Gamma}(\bar{\mathbf{r}}_v)$. The linear system that fuses the data from all the sub-apertures is obtained as in section 3.2, and the unknown matrix \mathbf{X} has six times more columns than in the acoustic case.

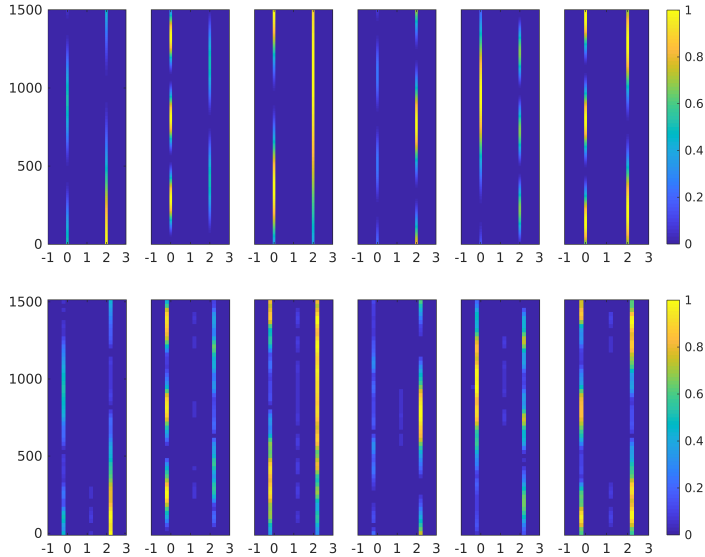


FIG. 4.2. Top line: From left to right we display all six components of the row vector $\mathbf{x}_{q\rightarrow}(\bar{\mathbf{r}})$ defined in (4.7), as a function of location along the aperture (the ordinate in meters) and cross-range location indexed by q in the imaging region (the abscissa, in units of $\lambda \bar{L}_o/A$). Bottom line: The MMV reconstruction.

Note that the approximation (4.5) of the Green's tensor $\hat{\mathcal{G}}(\omega, \mathbf{r}_j, \mathbf{y}_q)$ for the sub-aperture centered at $\bar{\mathbf{r}}$ has the one dimensional null space $\text{span}\{\bar{\mathbf{r}}\}$. This implies that the matrix $\mathbf{\Gamma}(\bar{\mathbf{r}})$ is also singular, so we cannot determine uniquely the reflectivity vectors $\boldsymbol{\rho}_{q\rightarrow}$ from equation (4.7). To be more explicit, we can represent the reflectivity tensor $\boldsymbol{\rho}_q$ in (4.4) in the sub-aperture dependent orthonormal basis $\{\mathbf{v}_j\}_{j=1,2,3}$ of eigenvectors of the matrix in (4.5), with $\mathbf{v}_3 = \bar{\mathbf{r}}/|\bar{\mathbf{r}}|$. Then, we obtain that the components $\{\mathbf{v}_j^T \boldsymbol{\rho}_q \mathbf{v}_l\}_{j=1,2,3}$ play no role in the data model (4.4), so we can only estimate $(\mathbf{v}_j^T \boldsymbol{\rho}_q \mathbf{v}_l)_{j,l=1,2}$. This ambiguity is due to the scaling relation $a/|\bar{\mathbf{r}}| \ll 1$ and it implies that only the transverse components of the electric field are needed in imaging, as the longitudinal component along \mathbf{v}_3 adds no information. If the reflectivity tensor does not change over directions, or it changes slowly, then the ambiguity can be overcome by taking into consideration the multiple sub-apertures, because $\bar{\mathbf{r}}$ changes orientation from one sub-aperture to another.

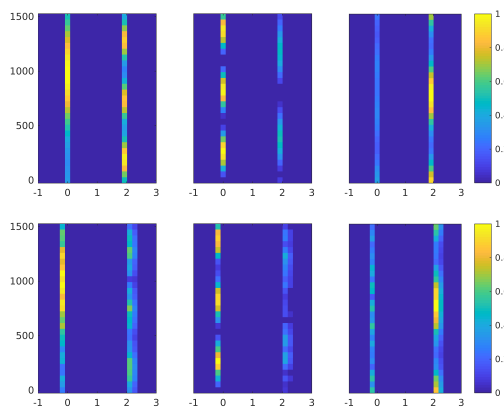


FIG. 4.3. Top line: The components $\mathbf{v}_j^T \boldsymbol{\rho}_q \mathbf{v}_l$ of the reflectivity matrix, for $j = l = 1$ (left plot), $j = l = 2$ (middle plot) and $j = 1, l = 2$ (right plot). The orthonormal basis $(\mathbf{v}_j)_{j=1,2,3}$ depends on the center location $\bar{\mathbf{r}}$ of the sub-aperture (the ordinate in meters). The abscissa is the cross-range location indexed by q , in units of $\lambda \bar{L}_o/A$. Bottom line: The reconstruction.

4.2. Numerical results. The setup for the numerical results is the same as in section 3.4. The data are generated using the single scattering model (4.1), for a reflectivity function that changes with the direction

of illumination and is supported at two points at distance of order $\bar{\lambda}\bar{L}_o/A$, where $\bar{L}_o = |\bar{\mathbf{r}}_o - \bar{\mathbf{y}}|$.

We display in Figure 4.2 the six entries of the row vectors $\mathbf{x}_{q \rightarrow}$ defined in (4.7), as $\bar{\mathbf{r}}$ varies in the large aperture, and for points in Ω indexed by q , separated by distances $\bar{\lambda}\bar{L}_o/A$ in cross-range. The plots in the bottom line of Figure 4.2 show that the MMV method gives good estimates of these row vectors.

In Figure 4.3 we display the components $(\mathbf{v}_j^T \boldsymbol{\rho}_q \mathbf{v}_l)_{j,l=1,2}$ of the reflectivity matrix $\boldsymbol{\rho}_q$ and its reconstruction, for each sub-aperture centered at $\bar{\mathbf{r}}$. As in the note at the end of the previous section, we let $\{\mathbf{v}_j\}_{j=1,2,3}$ be the orthonormal basis of eigenvectors of the approximation (4.5) of the Green's tensor, with \mathbf{v}_3 along $\bar{\mathbf{r}}$. The reconstruction displayed in Figure 4.3 is calculated as follows: With the estimated vectors $\mathbf{x}_{q \rightarrow}$ displayed in Figure 4.2 we calculate the minimum ℓ_2 norm solution of (4.7), using the truncated SVD of the singular matrix $\mathbf{\Gamma}(\bar{\mathbf{r}})$. This corresponds to setting to zero the components $\mathbf{v}_j^T \boldsymbol{\rho}_q \mathbf{v}_l$ of the estimated $\boldsymbol{\rho}_q$, for either j or l equal to 3. The other components are displayed in the figure, and they are well reconstructed.

5. Proofs. Here we prove the results stated in section 2.2. We begin with a Lemma, in section 5.1, which we then use in sections 5.2 and 5.3 to prove Theorems 2.1 and 2.2. Proposition 2.3 is proved in section 5.4 and the results for the clusters are proved in section 5.5.

5.1. A basic lemma. Let us denote by $\widehat{\mathbf{X}}$ the matrix obtained by normalizing the nonzero rows in \mathbf{X} , the unknown in the inverse problem, $\widehat{\mathbf{x}}_{q \rightarrow} = \frac{\mathbf{x}_{q \rightarrow}}{\|\mathbf{x}_{q \rightarrow}\|_2}$, for $q \in \mathcal{S}$. Introduce the linear operator

$$\mathfrak{L} : \mathbb{C}^{N_r \times N_v} \rightarrow \mathbb{C}, \quad \mathfrak{L}(\mathbf{V}) = \text{tr}[(\mathbf{G}\widehat{\mathbf{X}})^* \mathbf{V}], \quad \forall \mathbf{V} \in \mathbb{C}^{N_r \times N_v}, \quad (5.1)$$

where $\text{tr}[\cdot]$ denotes the trace. We have the following result:

LEMMA 5.1. *The linear operator \mathfrak{L} defined in (5.1) satisfies the inequality*

$$|\mathfrak{L}(\mathbf{V})| \leq \|(\mathbf{G}^* \mathbf{V})_{\mathcal{S}}\|_{1,2}, \quad (5.2)$$

for any $\mathbf{V} \in \mathbb{C}^{N_r \times N_v}$. The matrix \mathbf{X} satisfies the inequality

$$\|\mathbf{X}\|_{1,2}(1 - \mathcal{I}_{N_v}) \leq |\mathfrak{L}(\mathbf{G}\mathbf{X})|, \quad (5.3)$$

and with r , $\mathbf{X}^{\varepsilon,r}$ and $\mathbf{E}^{\varepsilon,r}$ defined as in Theorem 2.1, we have

$$|\mathfrak{L}(\mathbf{G}\mathbf{X}^{\varepsilon,r})| \leq (1 + \mathcal{I}_{N_v}) \|\mathbf{X}^{\varepsilon,r}\|_{1,2}, \quad (5.4)$$

$$|\mathfrak{L}(\mathbf{G}\mathbf{E}^{\varepsilon,r})| \leq (1 - r + \mathcal{I}_{N_v}) \|\mathbf{E}^{\varepsilon,r}\|_{1,2}. \quad (5.5)$$

Proof. We start with definition (5.1), and use the invariance of the trace under cyclic permutations, and the row support \mathcal{S} of \mathbf{X} , to obtain

$$\mathfrak{L}(\mathbf{G}\mathbf{X}) = \text{tr}[(\mathbf{G}\widehat{\mathbf{X}})^* \mathbf{G}\mathbf{X}] = \text{tr}[\mathbf{X}\widehat{\mathbf{X}}^* \mathbf{G}^* \mathbf{G}] = \sum_{j,q \in \mathcal{S}} (\mathbf{X}\widehat{\mathbf{X}}^*)_{j,q} (\mathbf{G}^* \mathbf{G})_{q,j} = \sum_{j,q \in \mathcal{S}} \langle \mathbf{x}_{j \rightarrow}, \widehat{\mathbf{x}}_{q \rightarrow} \rangle \langle \mathbf{g}_q, \mathbf{g}_j \rangle.$$

We rewrite this further with the normalization condition (2.14) and definition (2.12), and use the triangle inequality to obtain the bound

$$\begin{aligned} |\mathfrak{L}(\mathbf{G}\mathbf{X})| &= \left| \sum_{q \in \mathcal{S}} \left[\langle \mathbf{x}_{q \rightarrow}, \widehat{\mathbf{x}}_{q \rightarrow} \rangle \langle \mathbf{g}_q, \mathbf{g}_q \rangle + \sum_{j \in \mathcal{S} \setminus \{q\}} \langle \mathbf{x}_{j \rightarrow}, \widehat{\mathbf{x}}_{q \rightarrow} \rangle \langle \mathbf{g}_q, \mathbf{g}_j \rangle \right] \right| \\ &= \left| \sum_{q \in \mathcal{S}} \|\mathbf{x}_{q \rightarrow}\|_2 \left[1 + \sum_{j \in \mathcal{S} \setminus \{q\}} \mu(\mathbf{x}_{j \rightarrow}, \mathbf{x}_{q \rightarrow}) \mu(\mathbf{g}_q, \mathbf{g}_j) \right] \right| \\ &\geq \sum_{q \in \mathcal{S}} \|\mathbf{x}_{q \rightarrow}\|_2 \left[1 - \sum_{j \in \mathcal{S} \setminus \{q\}} |\mu(\mathbf{x}_{j \rightarrow}, \mathbf{x}_{q \rightarrow})| |\mu(\mathbf{g}_q, \mathbf{g}_j)| \right] \\ &\geq \sum_{q \in \mathcal{S}} \|\mathbf{x}_{q \rightarrow}\|_2 (1 - \mathcal{I}_{N_v}). \end{aligned}$$

The result (5.3) follows from definition of the matrix norm $\|\mathbf{X}\|_{1,2}$.

Similarly,

$$\mathfrak{L}(\mathbf{G}\mathbf{X}^{\varepsilon,r}) = \sum_{j \in \mathcal{S}^\varepsilon} \sum_{q \in \mathcal{S}} \langle \mathbf{x}_{j \rightarrow}^{\varepsilon,r}, \widehat{\mathbf{x}}_{q \rightarrow} \rangle \langle \mathbf{g}_q, \mathbf{g}_j \rangle = \sum_{j \in \mathcal{S}^\varepsilon} \|\mathbf{x}_{j \rightarrow}^{\varepsilon,r}\|_2 \sum_{q \in \mathcal{S}} \mu(\mathbf{x}_{j \rightarrow}^{\varepsilon,r}, \widehat{\mathbf{x}}_{q \rightarrow}) \mu(\mathbf{g}_q, \mathbf{g}_j),$$

where $\mathbf{x}_{j \rightarrow}^{\varepsilon,r}$ denotes the j -th row of $\mathbf{X}^{\varepsilon,r}$. Using the decomposition (2.27) of the row support \mathcal{S}^ε of $\mathbf{X}^{\varepsilon,r}$,

$$\begin{aligned} |\mathfrak{L}(\mathbf{G}\mathbf{X}^{\varepsilon,r})| &= \left| \sum_{i \in \mathcal{S}} \sum_{j \in \mathcal{S}_i^\varepsilon} \|\mathbf{x}_{j \rightarrow}^{\varepsilon,r}\|_2 \sum_{q \in \mathcal{S}} \mu(\mathbf{x}_{j \rightarrow}^{\varepsilon,r}, \widehat{\mathbf{x}}_{q \rightarrow}) \mu(\mathbf{g}_q, \mathbf{g}_j) \right| \\ &= \left| \sum_{i \in \mathcal{S}} \sum_{j \in \mathcal{S}_i^\varepsilon} \|\mathbf{x}_{j \rightarrow}^{\varepsilon,r}\|_2 \left[\mu(\mathbf{x}_{j \rightarrow}^{\varepsilon,r}, \widehat{\mathbf{x}}_{i \rightarrow}) \mu(\mathbf{g}_i, \mathbf{g}_j) + \sum_{q \in \mathcal{S} \setminus \{i\}} \mu(\mathbf{x}_{j \rightarrow}^{\varepsilon,r}, \widehat{\mathbf{x}}_{q \rightarrow}) \mu(\mathbf{g}_q, \mathbf{g}_j) \right] \right|. \end{aligned}$$

By the construction in (2.27), for any $j \in \mathcal{S}_i^\varepsilon$, the index $n(j) \in \mathcal{S}$ of the nearest point to \mathbf{y}_j is $n(j) = i$, so the sum in q is over the set $\mathcal{S} \setminus \{n(j)\}$. Using the triangle inequality and the definition (2.12) of \mathcal{I}_{N_v} , we get

$$\begin{aligned} |\mathfrak{L}(\mathbf{G}\mathbf{X}^{\varepsilon,r})| &\leq \sum_{i \in \mathcal{S}} \sum_{j \in \mathcal{S}_i^\varepsilon} \|\mathbf{x}_{j \rightarrow}^{\varepsilon,r}\|_2 \left[|\mu(\mathbf{x}_{j \rightarrow}^{\varepsilon,r}, \widehat{\mathbf{x}}_{i \rightarrow}) \mu(\mathbf{g}_i, \mathbf{g}_j)| + \sum_{q \in \mathcal{S} \setminus \{n(j)\}} |\mu(\mathbf{x}_{j \rightarrow}^{\varepsilon,r}, \widehat{\mathbf{x}}_{q \rightarrow}) \mu(\mathbf{g}_q, \mathbf{g}_j)| \right] \\ &\leq \sum_{i \in \mathcal{S}} \sum_{j \in \mathcal{S}_i^\varepsilon} \|\mathbf{x}_{j \rightarrow}^{\varepsilon,r}\|_2 (1 + \mathcal{I}_{N_v}) = \sum_{j \in \mathcal{S}^\varepsilon} \|\mathbf{x}_{j \rightarrow}^{\varepsilon,r}\|_2 (1 + \mathcal{I}_{N_v}). \end{aligned}$$

Since \mathcal{S}^ε is the row support of $\mathbf{X}^{\varepsilon,r}$, we can extend the sum to $1 \leq j \leq N_y$, and the result (5.4) follows from the definition of the $\|\cdot\|_{1,2}$ norm.

To prove (5.5), recall that $\mathbf{E}^{\varepsilon,r}$ is supported by definition in the set $\mathfrak{B}_r^c(\mathcal{S}) = \{1, \dots, N_y\} \setminus \mathfrak{B}_r(\mathcal{S})$. Then, if we denote by $\mathbf{e}_{j \rightarrow}^{\varepsilon,r}$ the rows of $\mathbf{E}^{\varepsilon,r}$, we have

$$\begin{aligned} \mathfrak{L}(\mathbf{G}\mathbf{E}^{\varepsilon,r}) &= \sum_{j \in \mathfrak{B}_r^c(\mathcal{S})} \sum_{q \in \mathcal{S}} \langle \mathbf{e}_{j \rightarrow}^{\varepsilon,r}, \widehat{\mathbf{x}}_{q \rightarrow} \rangle \langle \mathbf{g}_q, \mathbf{g}_j \rangle \\ &= \sum_{j \in \mathfrak{B}_r^c(\mathcal{S})} \|\mathbf{e}_{j \rightarrow}^{\varepsilon,r}\|_2 \sum_{q \in \mathcal{S}} \mu(\mathbf{e}_{j \rightarrow}^{\varepsilon,r}, \widehat{\mathbf{x}}_{q \rightarrow}) \mu(\mathbf{g}_q, \mathbf{g}_j) \\ &= \sum_{j \in \mathfrak{B}_r^c(\mathcal{S})} \|\mathbf{e}_{j \rightarrow}^{\varepsilon,r}\|_2 \left[\mu(\mathbf{e}_{j \rightarrow}^{\varepsilon,r}, \widehat{\mathbf{x}}_{n(j) \rightarrow}) \mu(\mathbf{g}_{n(j)}, \mathbf{g}_j) + \sum_{q \in \mathcal{S} \setminus \{n(j)\}} \mu(\mathbf{e}_{j \rightarrow}^{\varepsilon,r}, \widehat{\mathbf{x}}_{q \rightarrow}) \mu(\mathbf{g}_q, \mathbf{g}_j) \right]. \end{aligned}$$

Taking the absolute value and using the triangle inequality and definition (2.12) of \mathcal{I}_{N_v} , we obtain the bound

$$|\mathfrak{L}(\mathbf{G}\mathbf{E}^{\varepsilon,r})| \leq \sum_{j \in \mathfrak{B}_r^c(\mathcal{S})} \|\mathbf{e}_{j \rightarrow}^{\varepsilon,r}\|_2 \left[|\mu(\mathbf{e}_{j \rightarrow}^{\varepsilon,r}, \widehat{\mathbf{x}}_{n(j) \rightarrow}) \mu(\mathbf{g}_{n(j)}, \mathbf{g}_j)| + \mathcal{I}_{N_v} \right].$$

But $|\mu(\mathbf{e}_{j \rightarrow}^{\varepsilon,r}, \widehat{\mathbf{x}}_{n(j) \rightarrow})| \leq 1$ and $|\mu(\mathbf{g}_{n(j)}, \mathbf{g}_j)| = 1 - \mathfrak{D}(j, n(j))$, with $\mathfrak{D}(j, n(j)) \geq r$ for any $j \in \mathfrak{B}_r^c(\mathcal{S})$, so the bound becomes

$$|\mathfrak{L}(\mathbf{G}\mathbf{E}^{\varepsilon,r})| \leq \sum_{j \in \mathfrak{B}_r^c(\mathcal{S})} \|\mathbf{e}_{j \rightarrow}^{\varepsilon,r}\|_2 (1 - r + \mathcal{I}_{N_v}).$$

We can extend the sum to $1 \leq j \leq N_y$ because $\mathbf{E}^{\varepsilon,r}$ is supported in $\mathfrak{B}_r^c(\mathcal{S})$, and the result (5.5) follows from the definition of the $\|\cdot\|_{1,2}$ norm.

Finally, for any $\mathbf{V} \in \mathbb{C}^{N_r \times N_v}$, we obtain using the invariance of the trace to cyclic permutations that

$$\mathfrak{L}(\mathbf{V}) = \text{tr}[(\mathbf{G}\widehat{\mathbf{X}})^* \mathbf{V}] = \text{tr}[\mathbf{G}^* \mathbf{V} \widehat{\mathbf{X}}^*] = \sum_{j=1}^{N_y} \langle (\mathbf{G}^* \mathbf{V})_{j \rightarrow}, \widehat{\mathbf{x}}_{j \rightarrow} \rangle = \sum_{j \in \mathcal{S}} \langle (\mathbf{G}^* \mathbf{V})_{j \rightarrow}, \widehat{\mathbf{x}}_{j \rightarrow} \rangle,$$

where the last equality is because \mathbf{X} is row supported in \mathcal{S} . Taking the absolute value and using the triangle and Cauchy-Schwartz inequalities we get

$$|\mathfrak{L}(\mathbf{V})| \leq \sum_{j \in \mathcal{S}} |\langle (\mathbf{G}^* \mathbf{V})_{j \rightarrow}, \widehat{\mathbf{x}}_{j \rightarrow} \rangle| \leq \sum_{j \in \mathcal{S}} \|(\mathbf{G}^* \mathbf{V})_{j \rightarrow}\|_2 = \|(\mathbf{G}^* \mathbf{V})_{\mathcal{S} \rightarrow}\|_{1,2}.$$

This is the result (5.2) in the lemma. \square

5.2. Proof of Theorem 2.1. The bound (2.18) follows from the definition of \mathbf{W}^ε and the triangle inequality,

$$\|\mathbf{W}^\varepsilon\|_F = \|\mathbf{D}_\mathbf{W} - \mathbf{G}\mathbf{X}^\varepsilon - \mathbf{W}\|_F \leq \|\mathbf{D}_\mathbf{W} - \mathbf{G}\mathbf{X}^\varepsilon\|_F + \|\mathbf{W}\|_F \leq 2\varepsilon,$$

where we used the assumption (2.11) and that \mathbf{X}^ε is the minimizer of (2.10).

Using again the definition of \mathbf{W}^ε and the linearity of the operator (5.1), we write

$$\mathfrak{L}(\mathbf{G}\mathbf{X}) + \mathfrak{L}(\mathbf{W}^\varepsilon) = \mathfrak{L}(\mathbf{G}\mathbf{X} + \mathbf{W}^\varepsilon) = \mathfrak{L}(\mathbf{G}\mathbf{X}^\varepsilon) = \mathfrak{L}(\mathbf{G}\mathbf{X}^{\varepsilon,r}) + \mathfrak{L}(\mathbf{G}\mathbf{E}^{\varepsilon,r}),$$

where the last equality is by the decomposition (2.19). The result (5.3) in Lemma 5.1 gives

$$\|\mathbf{X}\|_{1,2}(1 - \mathcal{J}_{N_v}) \leq |\mathfrak{L}(\mathbf{G}\mathbf{X})| = |\mathfrak{L}(\mathbf{G}\mathbf{X}^{\varepsilon,r}) + \mathfrak{L}(\mathbf{G}\mathbf{E}^{\varepsilon,r}) - \mathfrak{L}(\mathbf{W}^\varepsilon)|,$$

and using the triangle inequality and the estimates (5.2), (5.4) and (5.5), we get

$$\begin{aligned} \|\mathbf{X}\|_{1,2}(1 - \mathcal{J}_{N_v}) &\leq |\mathfrak{L}(\mathbf{G}\mathbf{X}^{\varepsilon,r})| + |\mathfrak{L}(\mathbf{G}\mathbf{E}^{\varepsilon,r})| + |\mathfrak{L}(\mathbf{W}^\varepsilon)| \\ &\leq (1 + \mathcal{J}_{N_v})\|\mathbf{X}^{\varepsilon,r}\|_{1,2} + (1 - r + \mathcal{J}_{N_v})\|\mathbf{E}^{\varepsilon,r}\|_{1,2} + \|(\mathbf{G}^*\mathbf{W}^\varepsilon)_{\mathcal{S} \rightarrow}\|_{1,2}. \end{aligned} \quad (5.6)$$

Note that by (2.9) and (2.11),

$$\|\mathbf{G}\mathbf{X} - \mathbf{D}_\mathbf{W}\|_F = \|\mathbf{W}\|_F < \varepsilon,$$

so since \mathbf{X}^ε is the minimizer of (2.10), we must have $\|\mathbf{X}^\varepsilon\|_{1,2} \leq \|\mathbf{X}\|_{1,2}$. We also obtain from the decomposition (2.19) of \mathbf{X}^ε in the matrices $\mathbf{X}^{\varepsilon,r}$ and $\mathbf{E}^{\varepsilon,r}$ with disjoint row support that

$$\|\mathbf{X}^\varepsilon\|_{1,2} = \|\mathbf{X}^{\varepsilon,r} + \mathbf{E}^{\varepsilon,r}\|_{1,2} = \|\mathbf{X}^{\varepsilon,r}\|_{1,2} + \|\mathbf{E}^{\varepsilon,r}\|_{1,2}.$$

Substituting in (5.6) we get

$$\begin{aligned} \|\mathbf{X}^\varepsilon\|_{1,2}(1 - \mathcal{J}_{N_v}) &\leq (1 + \mathcal{J}_{N_v})(\|\mathbf{X}^\varepsilon\|_{1,2} - \|\mathbf{E}^{\varepsilon,r}\|_{1,2}) + (1 - r + \mathcal{J}_{N_v})\|\mathbf{E}^{\varepsilon,r}\|_{1,2} + \|(\mathbf{G}^*\mathbf{W}^\varepsilon)_{\mathcal{S} \rightarrow}\|_{1,2} \\ &= (1 + \mathcal{J}_{N_v})\|\mathbf{X}^\varepsilon\|_{1,2} - r\|\mathbf{E}^{\varepsilon,r}\|_{1,2} + \|(\mathbf{G}^*\mathbf{W}^\varepsilon)_{\mathcal{S} \rightarrow}\|_{1,2}. \end{aligned}$$

We also have from the definition of $\|\cdot\|_{1,2}$, the normalization of the columns of \mathbf{G} and (2.18), that

$$\|(\mathbf{G}^*\mathbf{W}^\varepsilon)_{\mathcal{S} \rightarrow}\|_{1,2} = \sum_{j \in \mathcal{S}} \|\mathbf{g}_j^* \mathbf{W}^\varepsilon\|_2 = \sum_{j \in \mathcal{S}} \left[\sum_{v=1}^{N_v} |\mathbf{g}_j^* \mathbf{w}_v^\varepsilon|^2 \right]^{1/2} \leq \sum_{j \in \mathcal{S}} \left[\sum_{v=1}^{N_v} \|\mathbf{w}_v^\varepsilon\|_2^2 \right]^{1/2} = |\mathcal{S}| \|\mathbf{W}^\varepsilon\|_F \leq 2\varepsilon |\mathcal{S}|, \quad (5.7)$$

where \mathbf{w}_v^ε are the columns of \mathbf{W}^ε . The result (2.20) stated in the theorem follows. \square

5.3. Proof of Theorem 2.2. Let us start with the definition of the matrices \mathbf{W}^ε , $\mathbf{X}^{\varepsilon,r}$ and $\mathbf{E}^{\varepsilon,r}$ given in Theorem 2.1, and write

$$\mathbf{G}\mathbf{X}^\varepsilon = \mathbf{G}(\mathbf{X}^{\varepsilon,r} + \mathbf{E}^{\varepsilon,r}) = \mathbf{G}\mathbf{X} + \mathbf{W}^\varepsilon.$$

With the decomposition (2.22) of $\mathbf{X}^{\varepsilon,r}$, we get

$$\mathbf{G}(\mathbf{X} - \mathfrak{X}^{\varepsilon,r}) = \mathbf{G}\mathbf{E}^{\varepsilon,r} + \mathbf{G}\mathfrak{E}^{\varepsilon,r} - \mathbf{W}^\varepsilon, \quad (5.8)$$

and we prove next the analogue of the result (5.6) for \mathbf{X} replaced by the matrix $\mathbf{X} - \mathfrak{X}^{\varepsilon,r}$ and $\mathbf{X}^{\varepsilon,r}$ replaced by 0. Looking at the proof of (5.3) in section 5.1, we note that we only used that \mathbf{X} has row support in \mathcal{S} . The same holds for the matrix $\mathbf{X} - \mathfrak{X}^{\varepsilon,r}$, so we can write directly the analogue of (5.3)

$$\|\mathbf{X} - \mathfrak{X}^{\varepsilon,r}\|_{1,2}(1 - \mathcal{J}_{N_v}) \leq \left| \mathfrak{L}(\mathbf{G}(\mathbf{X} - \mathfrak{X}^{\varepsilon,r})) \right|. \quad (5.9)$$

The right hand side in this equation can be estimated using (5.8) and the linearity of the operator \mathfrak{L} ,

$$\left| \mathfrak{L}\left(\mathbf{G}(\mathbf{X} - \mathfrak{X}^{\varepsilon,r})\right) \right| = \left| \mathfrak{L}(\mathbf{G}\mathbf{E}^{\varepsilon,r}) + \mathfrak{L}(\mathbf{G}\mathcal{E}^{\varepsilon,r} - \mathbf{W}^\varepsilon) \right| \leq \left| \mathfrak{L}(\mathbf{G}\mathbf{E}^{\varepsilon,r}) \right| + \left| \mathfrak{L}(\mathbf{G}\mathcal{E}^{\varepsilon,r} - \mathbf{W}^\varepsilon) \right|.$$

Substituting in (5.9) and using the estimates (5.5) and (5.2), with \mathbf{V} replaced by $\mathbf{G}\mathcal{E}^{\varepsilon,r} - \mathbf{W}^\varepsilon$, we obtain

$$\|\mathbf{X} - \mathfrak{X}^{\varepsilon,r}\|_{1,2}(1 - \mathcal{I}_{N_v}) \leq (1 - r + \mathcal{I}_{N_v})\|\mathbf{E}^{\varepsilon,r}\|_{1,2} + \left\| \left(\mathbf{G}^*(\mathbf{G}\mathcal{E}^{\varepsilon,r} - \mathbf{W}^\varepsilon)\right)_{\mathcal{S} \rightarrow} \right\|_{1,2}.$$

But, by equation (2.25),

$$\left(\mathbf{G}^*\mathbf{G}\mathcal{E}^{\varepsilon,r}\right)_{\mathcal{S} \rightarrow} = \mathbf{G}_S^*\mathbf{G}\mathcal{E}^{\varepsilon,r} = 0,$$

and the desired estimate is

$$\|\mathbf{X} - \mathfrak{X}^{\varepsilon,r}\|_{1,2}(1 - \mathcal{I}_{N_v}) \leq (1 - r + \mathcal{I}_{N_v})\|\mathbf{E}^{\varepsilon,r}\|_{1,2} + \left\| \left(\mathbf{G}^*\mathbf{W}^\varepsilon\right)_{\mathcal{S} \rightarrow} \right\|_{1,2}, \quad (5.10)$$

with the last term bounded as in (5.7).

Next, we substitute the bound (2.20) on the error term $\mathbf{E}^{\varepsilon,r}$ in (5.10), and obtain after simple algebraic manipulations that

$$\|\mathbf{X} - \mathfrak{X}^{\varepsilon,r}\|_{1,2} \leq \frac{2\mathcal{I}_{N_v}(1 - r + \mathcal{I}_{N_v})}{r(1 - \mathcal{I}_{N_v})}\|\mathbf{X}^\varepsilon\|_{1,2} + \frac{(1 + \mathcal{I}_{N_v})}{r(1 - \mathcal{I}_{N_v})}\left\| \left(\mathbf{G}^*\mathbf{W}^\varepsilon\right)_{\mathcal{S} \rightarrow} \right\|_{1,2}. \quad (5.11)$$

The assumption $2\mathcal{I}_{N_v} < r < 1$ implies that

$$1 - r + \mathcal{I}_{N_v} \leq 1 - 2\mathcal{I}_{N_v} + \mathcal{I}_{N_v} = 1 - \mathcal{I}_{N_v} \quad \text{and} \quad \frac{1 + \mathcal{I}_{N_v}}{1 - \mathcal{I}_{N_v}} < \frac{1 + \mathcal{I}_{N_v}}{1 - r/2} < 2(1 + \mathcal{I}_{N_v}) < 3.$$

Substituting in (5.11) we obtain the result (2.26) of Theorem 2.2.

It remains to prove the estimate (2.29). We begin with the identity

$$\mathfrak{X}^{\varepsilon,r} - \overline{\mathbf{X}^{\varepsilon,r}} = \mathbf{X}^{\varepsilon,r} - \overline{\mathbf{X}^{\varepsilon,r}} - \mathcal{E}^{\varepsilon,r},$$

and use equation (2.25) to conclude that

$$\mathbf{G}_S^*\mathbf{G}(\mathfrak{X}^{\varepsilon,r} - \overline{\mathbf{X}^{\varepsilon,r}}) = \mathbf{G}_S^*\mathbf{G}(\mathbf{X}^{\varepsilon,r} - \overline{\mathbf{X}^{\varepsilon,r}}).$$

By construction, both $\mathfrak{X}^{\varepsilon,r}$ and $\overline{\mathbf{X}^{\varepsilon,r}}$ are row supported in \mathcal{S} , so we can rewrite this equation as

$$\left(\mathfrak{X}^{\varepsilon,r} - \overline{\mathbf{X}^{\varepsilon,r}}\right)_{\mathcal{S} \rightarrow} - (\mathbf{I} - \mathbf{G}_S^*\mathbf{G}_S)\left(\mathfrak{X}^{\varepsilon,r} - \overline{\mathbf{X}^{\varepsilon,r}}\right)_{\mathcal{S} \rightarrow} = \mathbf{G}_S^*\mathbf{G}(\mathbf{X}^{\varepsilon,r} - \overline{\mathbf{X}^{\varepsilon,r}}), \quad (5.12)$$

where \mathbf{I} is the $|\mathcal{S}| \times |\mathcal{S}|$ identity matrix. We now estimate each term in this equation.

For the right hand side in (5.12) we have

$$\begin{aligned} \|\mathbf{G}_S^*\mathbf{G}(\mathbf{X}^{\varepsilon,r} - \overline{\mathbf{X}^{\varepsilon,r}})\|_{1,1} &= \sum_{q \in \mathcal{S}} \sum_{v=1}^{N_v} \left| \sum_{j=1}^{N_y} (\mathbf{G}_S^*\mathbf{G})_{q,j}(\mathbf{X}^{\varepsilon,r} - \overline{\mathbf{X}^{\varepsilon,r}})_{j,v} \right| \\ &= \sum_{q \in \mathcal{S}} \sum_{v=1}^{N_v} \left| \sum_{j \in \mathcal{S} \cup \mathcal{S}^\varepsilon} \mu(\mathbf{g}_q, \mathbf{g}_j)(\mathbf{X}^{\varepsilon,r} - \overline{\mathbf{X}^{\varepsilon,r}})_{j,v} \right| \\ &= \sum_{q \in \mathcal{S}} \sum_{v=1}^{N_v} \left| \sum_{j \in \mathcal{S} \cup \mathcal{S}^\varepsilon \setminus \mathcal{S}_q^\varepsilon} \mu(\mathbf{g}_q, \mathbf{g}_j)(\mathbf{X}^{\varepsilon,r} - \overline{\mathbf{X}^{\varepsilon,r}})_{j,v} + \sum_{j \in (\mathcal{S} \cup \mathcal{S}^\varepsilon) \cap \mathcal{S}_q^\varepsilon} \mu(\mathbf{g}_q, \mathbf{g}_j)(\mathbf{X}^{\varepsilon,r} - \overline{\mathbf{X}^{\varepsilon,r}})_{j,v} \right|, \end{aligned} \quad (5.13)$$

where the first two equalities are by the definition of the norm and of the matrix product, and the third equality uses the definition (2.13) and the row support $\mathcal{S} \cup \mathcal{S}^\varepsilon$ of $\mathbf{X}^{\varepsilon,r} - \overline{\mathbf{X}^{\varepsilon,r}}$. Now let us recall the definition (2.28) of $\overline{\mathbf{X}^{\varepsilon,r}}$, and the decomposition (2.27) of the support \mathcal{S}^ε of $\mathbf{X}^{\varepsilon,r}$, to obtain

$$\sum_{j \in (\mathcal{S} \cup \mathcal{S}^\varepsilon) \cap \mathcal{S}_q^\varepsilon} \mu(\mathbf{g}_q, \mathbf{g}_j) \mathbf{X}_{j,v}^{\varepsilon,r} = \sum_{j \in \mathcal{S}_q^\varepsilon} \mu(\mathbf{g}_q, \mathbf{g}_j) \mathbf{X}_{j,v}^{\varepsilon,r} = \overline{\mathbf{X}_{q,v}^{\varepsilon,r}} \quad \text{and} \quad \overline{\mathbf{X}_{j,v}^{\varepsilon,r}} = \overline{\mathbf{X}_{q,v}^{\varepsilon,r}} \delta_{j,q}, \quad \forall j \in \mathcal{S}_q^\varepsilon,$$

where $\delta_{j,q}$ is the Kronecker delta symbol. Since $\mu(\mathbf{g}_q, \mathbf{g}_q) = 1$, we conclude that the second term in (5.13) vanishes and the result becomes

$$\begin{aligned} \|\mathbf{G}_\mathcal{S}^* \mathbf{G}(\mathbf{X}^{\varepsilon,r} - \overline{\mathbf{X}^{\varepsilon,r}})\|_{1,1} &= \sum_{q \in \mathcal{S}} \sum_{v=1}^{N_v} \left| \sum_{j \in \mathcal{S} \cup \mathcal{S}^\varepsilon \setminus \mathcal{S}_q^\varepsilon} \mu(\mathbf{g}_q, \mathbf{g}_j) (\mathbf{X}^{\varepsilon,r} - \overline{\mathbf{X}^{\varepsilon,r}})_{j,v} \right| \\ &\leq \sum_{v=1}^{N_v} \sum_{q \in \mathcal{S}} \sum_{j \in \mathcal{S} \cup \mathcal{S}^\varepsilon \setminus \mathcal{S}_q^\varepsilon} |\mu(\mathbf{g}_q, \mathbf{g}_j)| \left| (\mathbf{X}^{\varepsilon,r} - \overline{\mathbf{X}^{\varepsilon,r}})_{j,v} \right|. \end{aligned} \quad (5.14)$$

Note that the set $\{(j, q) : j \in \mathcal{S} \cup \mathcal{S}^\varepsilon \setminus \mathcal{S}_q^\varepsilon, q \in \mathcal{S}\}$ is the same as the set $\{(j, q) : j \in \mathcal{S} \cup \mathcal{S}^\varepsilon, q \in \mathcal{S} \setminus \{n(j)\}\}$, so we can rewrite (5.14) as

$$\|\mathbf{G}_\mathcal{S}^* \mathbf{G}(\mathbf{X}^{\varepsilon,r} - \overline{\mathbf{X}^{\varepsilon,r}})\|_{1,1} \leq \sum_{v=1}^{N_v} \sum_{j \in \mathcal{S} \cup \mathcal{S}^\varepsilon} \left| (\mathbf{X}^{\varepsilon,r} - \overline{\mathbf{X}^{\varepsilon,r}})_{j,v} \right| \sum_{q \in \mathcal{S} \setminus \{n(j)\}} |\mu(\mathbf{g}_q, \mathbf{g}_j)|.$$

The last sum in this equation is bounded above by the interaction coefficient \mathcal{I}_1 , and using the definition of the $\|\cdot\|_{1,1}$ norm we get

$$\|\mathbf{G}_\mathcal{S}^* \mathbf{G}(\mathbf{X}^{\varepsilon,r} - \overline{\mathbf{X}^{\varepsilon,r}})\|_{1,1} \leq \mathcal{I}_1 \|\mathbf{X}^{\varepsilon,r} - \overline{\mathbf{X}^{\varepsilon,r}}\|_{1,1}. \quad (5.15)$$

With a similar calculation we obtain

$$\begin{aligned} \left\| (\mathbf{I} - \mathbf{G}_\mathcal{S}^* \mathbf{G}_\mathcal{S})(\mathbf{x}^{\varepsilon,r} - \overline{\mathbf{X}^{\varepsilon,r}}) \right\|_{1,1} &= \sum_{q \in \mathcal{S}} \sum_{v=1}^{N_v} \left| \sum_{j \in \mathcal{S}} (\mathbf{G}_\mathcal{S}^* \mathbf{G}_\mathcal{S} - \mathbf{I})_{q,j} (\mathbf{x}^{\varepsilon,r} - \overline{\mathbf{X}^{\varepsilon,r}})_{j,v} \right| \\ &\leq \sum_{j \in \mathcal{S}} \sum_{v=1}^{N_v} |(\mathbf{x}^{\varepsilon,r} - \overline{\mathbf{X}^{\varepsilon,r}})_{j,v}| \sum_{q \in \mathcal{S}} |\mu(\mathbf{g}_q, \mathbf{g}_j) - \delta_{q,j}| \\ &= \sum_{j \in \mathcal{S}} \sum_{v=1}^{N_v} |(\mathbf{x}^{\varepsilon,r} - \overline{\mathbf{X}^{\varepsilon,r}})_{j,v}| \sum_{q \in \mathcal{S} \setminus \{j\}} |\mu(\mathbf{g}_q, \mathbf{g}_j)|, \end{aligned}$$

where we used the triangle inequality, the identity $(\mathbf{G}_\mathcal{S}^* \mathbf{G}_\mathcal{S})_{q,j} = \mu(\mathbf{g}_q, \mathbf{g}_j)$ and $\mu(\mathbf{g}_q, \mathbf{g}_q) = 1$. The last sum is bounded above by the interaction coefficient \mathcal{I}_1 , and using that $\mathbf{x}^{\varepsilon,r} - \overline{\mathbf{X}^{\varepsilon,r}}$ is row supported in \mathcal{S} , and the definition of the $\|\cdot\|_{1,1}$ norm, we get

$$\left\| (\mathbf{I} - \mathbf{G}_\mathcal{S}^* \mathbf{G}_\mathcal{S})(\mathbf{x}^{\varepsilon,r} - \overline{\mathbf{X}^{\varepsilon,r}}) \right\|_{1,1} \leq \mathcal{I}_1 \|\mathbf{x}^{\varepsilon,r} - \overline{\mathbf{X}^{\varepsilon,r}}\|_{1,1}. \quad (5.16)$$

Gathering the results (5.12), (5.15)–(5.16), and using the triangle inequality, we obtain the bound

$$(1 - \mathcal{I}_1) \|\mathbf{x}^{\varepsilon,r} - \overline{\mathbf{X}^{\varepsilon,r}}\|_{1,1} \leq \mathcal{I}_1 \|\mathbf{X}^{\varepsilon,r} - \overline{\mathbf{X}^{\varepsilon,r}}\|_{1,1} \leq \mathcal{I}_1 \left(\|\mathbf{X}^{\varepsilon,r}\|_{1,1} + \|\overline{\mathbf{X}^{\varepsilon,r}}\|_{1,1} \right). \quad (5.17)$$

We also have from the definition (2.28) and the inequality $|\mu(\mathbf{g}_j, \mathbf{g}_l)| \leq 1$ for all $j, l = 1, \dots, N_y$, that

$$\|\overline{\mathbf{X}^{\varepsilon,r}}\|_{1,1} \leq \|\mathbf{X}^{\varepsilon,r}\|_{1,1}.$$

The estimate (2.29) in Theorem 2.2 follows by substituting this in (5.17). \square

5.4. Proof of Proposition 2.3. Recall from section 5.1 the definition of the unit row vectors $\widehat{\mathbf{x}}_{q\rightarrow}$. Because the rows of \mathbf{X} are assumed orthogonal in the proposition, $\{\widehat{\mathbf{x}}_{q\rightarrow}, q \in \mathcal{S}\}$ is an orthonormal subset of $\mathbb{C}^{1 \times N_v}$, and we conclude from Bessel's inequality that

$$\sum_{q \in \mathcal{S} \setminus \{n(j)\}} |\langle \mathbf{v}_{\rightarrow}, \widehat{\mathbf{x}}_{q\rightarrow} \rangle|^2 \leq \|\mathbf{v}_{\rightarrow}\|_2^2, \quad \forall \mathbf{v}_{\rightarrow} \in \mathbb{C}^{1 \times N_v} \text{ and } j = 1, \dots, N_{\mathbf{y}}.$$

Dividing both sides in this equation by $\|\mathbf{v}_{\rightarrow}\|_2^2$ and recalling definition (2.17), we obtain

$$\sum_{q \in \mathcal{S} \setminus \{n(j)\}} |\mu(\mathbf{v}_{\rightarrow}, \widehat{\mathbf{x}}_{q\rightarrow})|^2 \leq 1, \quad \forall \mathbf{v}_{\rightarrow} \in \mathbb{C}^{1 \times N_v} \text{ and } j = 1, \dots, N_{\mathbf{y}}. \quad (5.18)$$

For a given j and v , we define the vector $\boldsymbol{\nu}^{(j, \mathbf{v}_{\rightarrow})} \in \mathbb{R}^{1 \times (|\mathcal{S}|-1)}$ with entries $|\mu(\mathbf{v}_{\rightarrow}, \widehat{\mathbf{x}}_{q\rightarrow})|$. Recall also from section 2.2.4 the vector $\boldsymbol{\gamma}^{(j)} \in \mathbb{R}^{1 \times (|\mathcal{S}|-1)}$ with entries $|\mu(\mathbf{g}_j, \mathbf{g}_q)|$, for $q \in \mathcal{S} \setminus \{n(j)\}$, which is a set with cardinality $|\mathcal{S}| - 1$. Using these vectors, we have

$$\sup_{\mathbf{v}_{\rightarrow} \in \mathbb{C}^{1 \times N_v}} \sum_{q \in \mathcal{S} \setminus \{n(j)\}} |\mu(\mathbf{g}_j, \mathbf{g}_q)| |\mu(\mathbf{v}_{\rightarrow}, \widehat{\mathbf{x}}_{q\rightarrow})| = \sup_{\boldsymbol{\nu}^{(j, \mathbf{v}_{\rightarrow})} \in \mathbb{R}^{1 \times (|\mathcal{S}|-1)}, \|\boldsymbol{\nu}^{(j, \mathbf{v}_{\rightarrow})}\| \leq 1} \left(\boldsymbol{\nu}^{(j, \mathbf{v}_{\rightarrow})}, \boldsymbol{\gamma}^{(j)} \right) = \|\boldsymbol{\gamma}^{(j)}\|_2,$$

where (\cdot, \cdot) is the Euclidian inner product in $\mathbb{R}^{1 \times (|\mathcal{S}|-1)}$ and we used inequality (5.18) to conclude that $\boldsymbol{\nu}^{(j)}$ lies in the unit ball in $\mathbb{R}^{1 \times (|\mathcal{S}|-1)}$. The last equality is because the sup is achieved for $\boldsymbol{\nu}^{(j, \mathbf{v}_{\rightarrow})} = \boldsymbol{\gamma}^{(j)} / \|\boldsymbol{\gamma}^{(j)}\|_2$. Substituting in the definition (2.12), we obtain the result (2.30). \square

5.5. Proof of cluster results. The proof of Theorem 2.5 is the same as in section 5.2, with \mathbf{X} replaced by \mathbf{U} , \mathcal{S} replaced by \mathcal{C} and \mathbf{W} replaced by \mathbf{W} . This leads to the estimate

$$\|\mathbf{E}^{\varepsilon, r}\|_{1,2} \leq \frac{2\mathcal{J}_{N_v}^{\mathbf{U}}}{r} \|\mathbf{X}^{\varepsilon}\|_{1,2} + \frac{1}{r} \left\| (\mathbf{G}^* \mathbf{G} (\mathbf{X}^{\varepsilon} - \mathbf{X} + \mathbf{R}))_{\mathcal{C} \rightarrow} \right\|_{1,2} = \frac{2\mathcal{J}_{N_v}^{\mathbf{U}}}{r} \|\mathbf{X}^{\varepsilon}\|_{1,2} + \frac{1}{r} \left\| (\mathbf{G}^* \mathbf{W}^{\varepsilon})_{\mathcal{C} \rightarrow} \right\|_{1,2},$$

where we used that $\mathbf{U} = \mathbf{X} - \mathbf{R}$, the definition of \mathbf{W}^{ε} in Theorem 2.1 and $\mathbf{G}_{\mathcal{C}}^* \mathbf{G} \mathbf{R} = 0$. \square

It remains to prove Lemma 2.4. The projection (2.36) that defines \mathbf{U} induces the linear operator $\mathfrak{T} : \mathbb{C}^{N_r \times N_v} \rightarrow \mathbb{C}^{N_r \times N_v}$ that maps $\mathbf{G}\mathbf{U} = \mathfrak{T}\mathbf{G}\mathbf{X}$. Note that $\mathbf{G}\mathbf{U} = \mathfrak{T}\mathbf{G}\mathbf{U}$ and since

$$0 = \mathbf{G}_{\mathcal{C}}^* \mathbf{G} \mathbf{R} = \mathbf{G}_{\mathcal{C}}^* \mathbf{G} (\mathbf{X} - \mathbf{U}) = \mathbf{G}_{\mathcal{C}}^* (\mathbf{G}\mathbf{X} - \mathfrak{T}\mathbf{G}\mathbf{X}),$$

\mathfrak{T} is the orthogonal projection onto the range of $\mathbf{G}_{\mathcal{C}}$. To estimate

$$\|\mathbf{G}\mathbf{R}\|_F^2 = \|\mathbf{G}(\mathbf{X} - \mathbf{U})\|_F^2 = \sum_{v=1}^{N_v} \|\mathbf{G}(\mathbf{x}_v - \mathbf{u}_v)\|_2^2 = \sum_{v=1}^{N_v} \|\mathbf{G}\mathbf{x}_v - \mathfrak{T}\mathbf{G}\mathbf{x}_v\|_2^2, \quad (5.19)$$

we note that since \mathfrak{T} is the orthogonal projection on $\text{range}(\mathbf{G}_{\mathcal{C}})$,

$$\|\mathbf{G}\mathbf{x}_v - \mathfrak{T}\mathbf{G}\mathbf{x}_v\|_2 \leq \|\mathbf{G}\mathbf{x}_v - \mathbf{z}\|_2, \quad \forall \mathbf{z} \in \text{range}(\mathbf{G}_{\mathcal{C}}). \quad (5.20)$$

Now let us define the "effective cluster matrix" $\overline{\mathbf{X}}$, with entries

$$\overline{\mathbf{X}}_{j,v} = \begin{cases} \sum_{l \in \mathcal{S}_j} \mathbf{X}_{l,v} \mu(\mathbf{g}_j, \mathbf{g}_l), & j \in \mathcal{C}, \\ 0, & \text{otherwise,} \end{cases} \quad \text{for } 1 \leq j \leq N_{\mathbf{y}}, 1 \leq v \leq N_v. \quad (5.21)$$

We use the inequality (5.20) for $\mathbf{z} = \mathbf{G}\overline{\mathbf{X}} = \mathbf{G}_{\mathcal{C}}\overline{\mathbf{X}}_{\mathcal{C} \rightarrow}$, and obtain

$$\|\mathbf{G}\mathbf{x}_v - \mathfrak{T}\mathbf{G}\mathbf{x}_v\|_2 \leq \|\mathbf{G}\mathbf{x}_v - \mathbf{G}\overline{\mathbf{x}}_v\|_2 = \left\| \sum_{j \in \mathcal{S}} X_{j,v} \mathbf{g}_j - \sum_{j \in \mathcal{C}} \overline{X}_{j,v} \mathbf{g}_j \right\|_2, \quad (5.22)$$

because \mathbf{X} is row supported in \mathcal{S} and $\overline{\mathbf{X}}$ is row supported in \mathcal{C} . Next, using the decomposition (2.37) of \mathcal{S} and the definition (5.21) of $\overline{\mathbf{X}}$, we have

$$\begin{aligned} \left\| \sum_{j \in \mathcal{S}} X_{j,v} \mathbf{g}_j - \sum_{j \in \mathcal{C}} \overline{X}_{j,v} \mathbf{g}_j \right\|_2 &= \left\| \sum_{j \in \mathcal{C}} \sum_{l \in \mathcal{S}_j} X_{l,v} \mathbf{g}_l - \sum_{j \in \mathcal{C}} \left[\sum_{l \in \mathcal{S}_j} X_{l,v} \mu(\mathbf{g}_j, \mathbf{g}_l) \right] \mathbf{g}_j \right\|_2 \\ &= \left\| \sum_{j \in \mathcal{C}} \sum_{l \in \mathcal{S}_j} X_{l,v} [\mathbf{g}_l - \mu(\mathbf{g}_j, \mathbf{g}_l) \mathbf{g}_j] \right\|_2. \end{aligned} \quad (5.23)$$

We can bound this using the triangle inequality and

$$\left\| \mathbf{g}_l - \mu(\mathbf{g}_j, \mathbf{g}_l) \mathbf{g}_j \right\|_2^2 = \langle \mathbf{g}_l - \mu(\mathbf{g}_j, \mathbf{g}_l) \mathbf{g}_j, \mathbf{g}_l - \mu(\mathbf{g}_j, \mathbf{g}_l) \mathbf{g}_j \rangle = 1 - |\mu(j, l)|^2 \leq 2\mathfrak{D}(j, l), \quad (5.24)$$

where we used the definition of the semimetric \mathfrak{D} and of μ . Since \mathcal{S}_j is contained within a ball of radius r_c centered at $j \in \mathcal{C}$, we have $\mathfrak{D}(j, l) \leq r_c$ in (5.24), and gathering the results (5.22)–(5.24), we get

$$\left\| \mathbf{G} \mathbf{x}_v - \mathfrak{T} \mathbf{G} \mathbf{x}_v \right\|_2 \leq \sqrt{2r_c} \sum_{j \in \mathcal{C}} \sum_{l \in \mathcal{S}_j} |X_{l,v}| = \sqrt{2r_c} \|\mathbf{x}_v\|_1. \quad (5.25)$$

Finally, substituting in (5.19),

$$\|\mathbf{G} \mathbf{R}\|_F^2 \leq 2r_c \sum_{v=1}^{N_v} (\|\mathbf{x}_v\|_1)^2 = 2r_c \|\mathbf{X}^T\|_{2,1}^2. \quad \square$$

6. Summary. We presented a novel resolution theory for synthetic aperture radar (SAR) imaging using the multiple measurement vector (MMV) approach, also known as simultaneously sparse optimization. This seeks to find an unknown matrix \mathbf{X} with sparse row support, by inverting a linear system of equations using sparsity promoting convex optimization. In the SAR imaging application, \mathbf{X} models the unknown reflectivity of a scattering scene. The rows of \mathbf{X} are indexed by the points in the imaging region, and the columns correspond to its values for multiple views of the imaging scene, from different sub-apertures and polarization diverse measurements.

The resolution theory does not pursue the question of exact recovery, but seeks to estimate the neighborhood of the support of \mathbf{X} where the largest entries in the reconstruction lie. The radius of this neighborhood represents the resolution limit and it depends on the noise level. We introduced a quantifier of how the unknowns influence each other in imaging, called the multiple view interaction coefficient, and showed that the smaller this is and the weaker the noise, the better the estimate of the support of \mathbf{X} . We also quantified the error of the reconstruction and studied the advantage of having multiple views. The existing literature shows that the MMV method does not always perform better than sparsity promoting optimization with a single view, the so-called single measurement vector (SMV) formulation. We showed that if the rows of \mathbf{X} are orthogonal, then the MMV approach is expected to perform better, depending on how the unknowns are distributed in the imaging scene. We quantified this advantage and explained how the condition of orthogonality of the rows of \mathbf{X} arises in the application of SAR imaging of direction dependent reflectivity.

We also studied imaging of well-separated clusters of scatterers and showed that the MMV approach gives a reconstruction supported near these clusters.

Acknowledgments. This material is based upon work supported by the Air Force Office of Scientific Research under award number FA9550-15-1-0118.

Appendix A. Proof of Proposition 3.1. Let us introduce the notation

$$\xi_{q,v} = \rho_q(\bar{\mathbf{r}}_v, \omega) \sqrt{N_r} \varphi \left[b \left(\bar{t} + \frac{2\mathbf{m}_1 \cdot \Delta \mathbf{y}_q}{c} \right) \right]. \quad (A.1)$$

Assuming that φ is smooth and using that the spacing between the centers of consecutive sub-apertures is small, we approximate the correlation of the rows of \mathbf{X} by

$$\left| \mu(\mathbf{x}_{q \rightarrow}, \mathbf{x}_{l \rightarrow}) \right| \approx \frac{\left| \int_{-A/2}^{A/2} dr \psi_{q,l}(r) \exp \left[2i\bar{k} \frac{(\mathbf{r}_o + r\boldsymbol{\tau} - \bar{\mathbf{y}})}{|\mathbf{r}_o + r\boldsymbol{\tau} - \bar{\mathbf{y}}|} \cdot (\mathbf{y}_q - \mathbf{y}_l) \right] \right|}{\|\psi_{q,q}\|_{L_1(-A/2, A/2)}^{1/2} \|\psi_{l,l}\|_{L_1(-A/2, A/2)}^{1/2}}. \quad (A.2)$$

Recall that \mathbf{r}_o is the center of the large linear aperture, along $\boldsymbol{\tau}$. We parametrize this aperture by the arclength $r \in [-A/2, A/2]$, and $\psi_{q,l}(r)$ is the smooth kernel satisfying the interpolation conditions

$$\psi_{q,l} \left(r = \left(\frac{v-1}{N_v-1} - \frac{1}{2} \right) A \right) = \xi_{q,v} \xi_{l,v}^*. \quad (\text{A.3})$$

To estimate (A.2) we expand the exponent in r

$$\bar{k} \frac{(\mathbf{r}_o + r\boldsymbol{\tau} - \bar{\mathbf{y}})}{|\mathbf{r}_o + r\boldsymbol{\tau} - \bar{\mathbf{y}}|} \cdot (\mathbf{y}_q - \mathbf{y}_l) = \bar{k} \mathbf{m}_o \cdot (\mathbf{y}_q - \mathbf{y}_l) + \bar{k} r \frac{\boldsymbol{\tau} \cdot \mathbb{P}_o(\mathbf{y}_q - \mathbf{y}_l)}{|\mathbf{r}_o - \bar{\mathbf{y}}|} + \dots, \quad (\text{A.4})$$

with \mathbf{m}_o and \mathbb{P}_o defined as in Proposition 3.1. Suppose that A and the cross-range offset between \mathbf{y}_q and \mathbf{y}_l are small enough so we can neglect the higher terms^{||} in (A.4). Then, using Q defined in Proposition 3.1 and integrating by parts in (A.2), we obtain

$$|\mu(\mathbf{x}_{q \rightarrow}, \mathbf{x}_{l \rightarrow})| \approx \frac{A \left| \psi_{q,l}(A/2) e^{iQ/2} - \psi_{q,l}(-A/2) e^{-iQ/2} - \int_{-A/2}^{A/2} dr \psi'_{q,l}(r) e^{irQ/A} \right|}{|Q| \|\psi_{q,q}\|_{L_1(-A/2, A/2)}^{1/2} \|\psi_{l,l}\|_{L_1(-A/2, A/2)}^{1/2}}. \quad (\text{A.5})$$

If the reflectivities are independent of direction, (A.5) becomes $|\mu(\mathbf{x}_{q \rightarrow}, \mathbf{x}_{l \rightarrow})| \approx |\text{sinc}(Q/2)|$. This attains its maximum at $Q = 0$ i.e., at $q = l$, and decays as $1/|Q|$, as stated in the proposition. It remains to show that the result extends to reflectivities that vary smoothly with direction. We obtain from (A.5), using the triangle inequality, that

$$|\mu(\mathbf{x}_{q \rightarrow}, \mathbf{x}_{l \rightarrow})| \leq \frac{A \left[|\psi_{q,l}(A/2)| + |\psi_{q,l}(-A/2)| + \|\psi'_{q,l}\|_{L_1(-A/2, A/2)} \right]}{|Q| \|\psi_{q,q}\|_{L_1(-A/2, A/2)}^{1/2} \|\psi_{l,l}\|_{L_1(-A/2, A/2)}^{1/2}}, \quad (\text{A.6})$$

and we estimate next the three terms in the numerator. We begin with

$$|\psi_{q,l}(A/2)| \leq |\psi_{q,l}(s)| + \left| \int_s^{A/2} dr \psi'_{q,l}(r) \right|,$$

where we used the fundamental theorem of calculus and the triangle inequality. Therefore,

$$\begin{aligned} A |\psi_{q,l}(A/2)| &= \int_{-A/2}^{A/2} ds |\psi_{q,l}(A/2)| \leq \int_{-A/2}^{A/2} ds |\psi_{q,l}(s)| + \int_{-A/2}^{A/2} ds \left| \int_s^{A/2} dr \psi'_{q,l}(r) \right| \\ &\leq \|\psi_{q,l}\|_{L_1(-A/2, A/2)} + \int_{-A/2}^{A/2} ds \int_{-A/2}^{A/2} dr |\psi'_{q,l}(r)| \\ &= \|\psi_{q,l}\|_{L_1(-A/2, A/2)} + A \|\psi'_{q,l}\|_{L_1(-A/2, A/2)}. \end{aligned} \quad (\text{A.7})$$

The first term in this equation can be bound using the Cauchy-Schwartz inequality, once we recall the definition (A.3) of $\psi_{q,l}$. We rewrite this definition as

$$\psi_{q,l}(r) = \xi_q(\mathbf{r}_o + r\boldsymbol{\tau}) \xi_l^*(\mathbf{r}_o + r\boldsymbol{\tau}), \quad (\text{A.8})$$

in an abuse of notation, so that $\xi_{q,v} = \xi_q(\mathbf{r}_v)$, for $\mathbf{r}_v = \mathbf{r}_o + \left(\frac{v-1}{N_v-1} - \frac{1}{2} \right) A\boldsymbol{\tau}$. We obtain that

$$\begin{aligned} L_2 \|\psi_{q,l}\|_{L_1(-A/2, A/2)} &= \int_{-A/2}^{A/2} dr |\xi_q(\mathbf{r}_o + r\boldsymbol{\tau}) \xi_l^*(\mathbf{r}_o + r\boldsymbol{\tau})| \\ &\leq \left[\int_{-A/2}^{A/2} dr |\xi_q(\mathbf{r}_o + r\boldsymbol{\tau})|^2 \right]^{1/2} \left[\int_{-A/2}^{A/2} dr |\xi_l(\mathbf{r}_o + r\boldsymbol{\tau})|^2 \right]^{1/2} \\ &= \|\psi_{q,q}\|_{L_1(-A/2, A/2)}^{1/2} \|\psi_{l,l}\|_{L_1(-A/2, A/2)}^{1/2}. \end{aligned}$$

^{||}The results are qualitatively the same if we include quadratic terms in r and neglect cubic and higher order terms. The discussion is simpler if we consider only the shown terms in (A.4).

We also have from (A.8) that

$$\psi'_{q,l}(r) = \boldsymbol{\tau} \cdot \nabla \xi_q(\mathbf{r}_o + r\boldsymbol{\tau}) \xi_l^*(\mathbf{r}_o + r\boldsymbol{\tau}) + \xi_q(\mathbf{r}_o + r\boldsymbol{\tau}) \boldsymbol{\tau} \cdot \nabla \xi_l^*(\mathbf{r}_o + r\boldsymbol{\tau}),$$

and from the Cauchy-Schwartz and triangle inequalities we get

$$\begin{aligned} \|\psi'_{q,l}\|_{L_1(-A/2,A/2)} &\leq \|\boldsymbol{\tau} \cdot \nabla \xi_q\|_{L_2(-A/2,A/2)} \|\xi_l\|_{L_2(-A/2,A/2)} + \|\xi_q\|_{L_2(-A/2,A/2)} \|\boldsymbol{\tau} \cdot \nabla \xi_l\|_{L_2(-A/2,A/2)} \\ &\leq \|\nabla \xi_q\|_{L_2(-A/2,A/2)} \|\xi_l\|_{L_2(-A/2,A/2)} + \|\xi_q\|_{L_2(-A/2,A/2)} \|\nabla \xi_l\|_{L_2(-A/2,A/2)}. \end{aligned}$$

To estimate this further, let us introduce the constant K_q , which depends on the scale of variation of the reflectivity ξ_q , such that

$$\|\nabla \xi_q\|_{L_2(-A/2,A/2)} \leq \frac{K_q}{A} \|\xi_q\|_{L_2(-A/2,A/2)}.$$

Since $\|\xi_q\|_{L_2(-A/2,A/2)} = \|\psi_{q,q}\|_{L_1(-A/2,A/2)}^{1/2}$ by definition (A.8), we obtain that

$$A \|\psi'_{q,l}\|_{L_1(-A/2,A/2)} \leq (K_q + K_l) \|\psi_{q,q}\|_{L_1(-A/2,A/2)}^{1/2} \|\psi_{l,l}\|_{L_1(-A/2,A/2)}^{1/2}.$$

The estimate (A.7) becomes

$$A |\psi_{q,l}(A/2)| \leq (1 + K_q + K_l) \|\psi_{q,q}\|_{L_1(-A/2,A/2)}^{1/2} \|\psi_{l,l}\|_{L_1(-A/2,A/2)}^{1/2},$$

and a similar bound applies to $A |\psi_{q,l}(-A/2)|$. Gathering the results and substituting in (A.6), we obtain the statement of the proposition, with $C_{q,l} = 12\pi(1 + K_q + K_l)$. \square

Appendix B. Expression of matrix $\mathbf{\Gamma}(\bar{\mathbf{r}})$. The 6×6 matrix $\mathbf{\Gamma}(\bar{\mathbf{r}})$ that enters the data model (4.6) can be written as

$$\mathbf{\Gamma}(\bar{\mathbf{r}}) = \mathbf{\Gamma}_{\text{diag}}(\bar{\mathbf{r}}) + \mathbf{\Gamma}_{\text{off-diag}}(\bar{\mathbf{r}})$$

where

$$\begin{aligned} \mathbf{\Gamma}_{\text{diag}}(\bar{\mathbf{r}}) = \text{diagonal} &\left((1 - \eta_1^2)^2, (1 - \eta_2^2)^2, (1 - \beta^2)^2, (1 - \eta_1^2)(1 - \eta_2^2) + (\eta_1 \eta_2)^2, \right. \\ &\left. (1 - \eta_1^2)(1 - \beta^2) + (\eta_1 \beta)^2, (1 - \eta_2^2)(1 - \beta^2) + (\eta_2 \beta)^2 \right), \end{aligned}$$

is the diagonal part of $\mathbf{\Gamma}(\bar{\mathbf{r}})$ and

$$\mathbf{\Gamma}_{\text{off-diag}}(\bar{\mathbf{r}}) = \begin{pmatrix} 0 & (\eta_1 \eta_2)^2 & (\eta_1 \beta)^2 & \eta_1 \eta_2 (\eta_1^2 - 1) & \eta_1 \beta (\eta_1^2 - 1) & \eta_1^2 \eta_2 \beta \\ (\eta_1 \eta_2)^2 & 0 & (\eta_2 \beta)^2 & \eta_1 \eta_2 (\eta_2^2 - 1) & \eta_1 \eta_2^2 \beta & \eta_2 \beta (\eta_2^2 - 1) \\ (\eta_1 \beta)^2 & (\eta_2 \beta)^2 & 0 & \eta_1 \eta_2 \beta^2 & \eta_1 \beta (\beta^2 - 1) & \eta_2 \beta (\beta^2 - 1) \\ 2\eta_1 \eta_2 (\eta_1^2 - 1) & 2\eta_1 \eta_2 (\eta_2^2 - 1) & 2\eta_1 \eta_2 \beta^2 & 0 & \eta_2 \beta (2\eta_1^2 - 1) & \eta_1 \beta (2\eta_2^2 - 1) \\ 2\eta_1 \beta (\eta_1^2 - 1) & 2\eta_1 \eta_2^2 \beta & 2\eta_1 \beta (\beta^2 - 1) & \eta_2 \beta (2\eta_1^2 - 1) & 0 & \eta_1 \eta_2 (2\beta^2 - 1) \\ 2\eta_1^2 \eta_2 \beta & 2\eta_2 \beta (\eta_2^2 - 1) & 2\eta_2 \beta (\beta^2 - 1) & \eta_1 \beta (2\eta_2^2 - 1) & \eta_1 \eta_2 (2\beta^2 - 1) & 0 \end{pmatrix}$$

is its off-diagonal part.

REFERENCES

- [1] *GOTCHA volumetric SAR data set*. <https://www.sdms.afrl.af.mil/index.php?collection=gotcha>.
- [2] H. AMMARI, J. GARNIER, W. JINGAND H. KANG, M. LIM, K. SÖLNA, AND H. WANG, *Mathematical and statistical methods for multistatic imaging*, vol. 2098, Springer, 2013.
- [3] H. AMMARI, E. IAKOVLEVA, D. LESSELIER, AND G. PERRUSSON, *MUSIC-type electromagnetic imaging of a collection of small three-dimensional inclusions*, *SIAM Journal on Scientific Computing*, 29 (2007), pp. 674–709.
- [4] R. BARANIUK AND P. STEEGHS, *Compressive radar imaging*, in *Radar Conference, 2007 IEEE*, IEEE, 2007, pp. 128–133.
- [5] B. BIONDI, *3D seismic imaging*, Society of Exploration Geophysicists, 2006.
- [6] J. BOBIN, J-L STARCK, AND R. OTTENSAMER, *Compressed sensing in astronomy*, *IEEE Journal of Selected Topics in Signal Processing*, 2 (2008), pp. 718–726.

- [7] L. BORCEA AND I. KOCYIGIT, *Resolution analysis of imaging with ℓ_1 optimization*, SIAM Journal on Imaging Sciences, 8 (2015), pp. 3015–3050.
- [8] L. BORCEA, M. MOSCOSO, G. C. PAPANICOLAOU, AND C. TSOGKA, *Synthetic aperture imaging of direction-and frequency-dependent reflectivities*, SIAM Journal on Imaging Sciences, 9 (2016), pp. 52–81.
- [9] A. M. BRUCKSTEIN, D. L. DONOHO, AND M. ELAD, *From sparse solutions of systems of equations to sparse modeling of signals and images*, SIAM review, 51 (2009), pp. 34–81.
- [10] E. J. CANDÈS, J. ROMBERG, AND T. TAO, *Robust uncertainty principles: Exact signal reconstruction from highly incomplete frequency information*, IEEE Transactions on information theory, 52 (2006), pp. 489–509.
- [11] E. J. CANDÈS AND T. TAO, *Decoding by linear programming*, Information Theory, IEEE Transactions on, 51 (2005), pp. 4203–4215.
- [12] ———, *Near-optimal signal recovery from random projections: Universal encoding strategies?*, IEEE transactions on information theory, 52 (2006), pp. 5406–5425.
- [13] A. CHAI, M. MOSCOSO, AND G. PAPANICOLAOU, *Robust imaging of localized scatterers using the singular value decomposition and l_1 minimization*, Inverse Problems, 29 (2013), p. 025016.
- [14] ———, *Imaging strong localized scatterers with sparsity promoting optimization*, SIAM Journal on Imaging Sciences, 7 (2014), pp. 1358–1387.
- [15] J. CHEN AND X. HUO, *Theoretical results on sparse representations of multiple-measurement vectors*, IEEE Transactions on Signal Processing, 54 (2006), pp. 4634–4643.
- [16] M. CHENEY, *Imaging frequency-dependent reflectivity from synthetic-aperture radar*, Inverse Problems, 29 (2013), p. 054002.
- [17] M. CHENEY AND B. BORDEN, *Fundamentals of radar imaging*, SIAM, 2009.
- [18] A. COHEN, W. DAHMEN, AND R. DEVORE, *Compressed sensing and best k -term approximation*, J. Amer. Math. Soc. (2009), pp. 211–231.
- [19] S. F. COTTER, B. D. RAO, K. ENGAN, AND K. KREUTZ-DELGADO, *Sparse solutions to linear inverse problems with multiple measurement vectors*, Signal Processing, IEEE Transactions on, 53 (2005), pp. 2477–2488.
- [20] J. C. CURLANDER AND R. N. MCDONOUGH, *Synthetic aperture radar*, John Wiley & Sons New York, NY, USA, 1991.
- [21] CVX RESEARCH, *Cvx: matlab software for disciplined convex programming, version 2.0*. <http://cvxr.com/cvx><http://cvxr.com/cvx>, August 2012.
- [22] D. L. DONOHO, *Compressed sensing*, IEEE Transactions on information theory, 52 (2006), pp. 1289–1306.
- [23] D. L. DONOHO AND M. ELAD, *Optimally sparse representation in general (nonorthogonal) dictionaries via l_1 minimization*, Proceedings of the National Academy of Sciences, 100 (2003), pp. 2197–2202.
- [24] D. L. DONOHO AND X. HUO, *Uncertainty principles and ideal atomic decomposition*, IEEE Trans. Inf. Theor., 47 (2006), pp. 2845–2862.
- [25] D. L. DONOHO AND B. F. LOGAN, *Signal recovery and the large sieve*, SIAM Journal on Applied Mathematics, 52 (1992), pp. 577–591.
- [26] D. L. DONOHO AND P. B. STARK, *Uncertainty principles and signal recovery*, SIAM Journal on Applied Mathematics, 49 (1989), pp. 906–931.
- [27] Y. C. ELДАР AND M. MISHALI, *Robust recovery of signals from a structured union of subspaces*, IEEE Transactions on Information Theory, 55 (2009), pp. 5302–5316.
- [28] A. FANJANG AND H-C TSENG, *Compressive radar with off-grid targets: a perturbation approach*, Inverse Problems, 29 (2013), p. 054008.
- [29] A. C. FANJANG, T. STROHMER, AND P. YAN, *Compressed remote sensing of sparse objects*, SIAM Journal on Imaging Sciences, 3 (2010), pp. 595–618.
- [30] M. LUSTIG, D. L. DONOHO, AND J. M. PAULY, *Sparse mri: The application of compressed sensing for rapid mr imaging*, Magnetic resonance in medicine, 58 (2007), pp. 1182–1195.
- [31] D. MALIOUTOV, M. CETIN, AND A. S. WILLSKY, *A sparse signal reconstruction perspective for source localization with sensor arrays*, IEEE Transactions on Signal Processing, 53 (2005), pp. 3010–3022.
- [32] L. C. POTTER, E. ERTIN, J. T. PARKER, AND M. CETIN, *Sparsity and compressed sensing in radar imaging*, Proceedings of the IEEE, 98 (2010), pp. 1006–1020.
- [33] F. SANTOSA AND W. W. SYMES, *Linear inversion of band-limited reflection seismograms*, SIAM Journal on Scientific and Statistical Computing, 7 (1986), pp. 1307–1330.
- [34] P. SOTIRELIS, J. PARKER, X. HU, M. CHENEY, AND M. FERRARA, *Frequency-dependent reflectivity image reconstruction*, in SPIE Defense, Security, and Sensing, International Society for Optics and Photonics, 2013, pp. 874602–874602.
- [35] P. SOTIRELIS, J. T. PARKER, M. FU, X. HU, AND R. ALBANESE, *A study of material identification using SAR*, in Radar Conference (RADAR), 2012 IEEE, IEEE, 2012, pp. 0112–0115.
- [36] J. A. TROPP, *Greed is good: Algorithmic results for sparse approximation*, Information Theory, IEEE Transactions on, 50 (2004), pp. 2231–2242.
- [37] ———, *Algorithms for simultaneous sparse approximation: Part ii: Convex relaxation*, Signal Process., 86 (2006), pp. 589–602.
- [38] J. A. TROPP, A. C. GILBERT, AND M. J. STRAUSS, *Algorithms for simultaneous sparse approximation: Part i: Greedy pursuit*, Signal Process., 86 (2006), pp. 572–588.
- [39] E. VAN DEN BERG AND M. P. FRIEDLANDER, *Theoretical and empirical results for recovery from multiple measurements*, IEEE Transactions on Information Theory, 56 (2010), pp. 2516–2527.